

Response and Recovery of Horn and Petit Bois Islands, Mississippi, USA to Tropical Cyclone Impacts: 2004 - 2016

Shara L. Gremillion, shara.gremillion@usm.edu
Davin J. Wallace, davin.wallace@usm.edu (corresponding author)
Samuel L. Wright, slwcoin@gmail.com
Maarten C. Buijsman, maarten.buijsman@usm.edu

School of Ocean Science and Engineering, University of Southern Mississippi, Stennis Space Center, MS 39529, USA

Corresponding author information:

Davin Wallace, davin.wallace@usm.edu (Phone) 228-688-3060, (Fax) 228-688-1121
School of Ocean Science and Engineering, University of Southern Mississippi, 1020 Balch Blvd., Stennis Space Center, MS 39529, USA

ABSTRACT

1
2 Horn and Petit Bois islands are two of five Mississippi (MS) barrier islands that provide
3 physical protection from tropical cyclones threatening the MS Gulf Coast, in addition to critical
4 habitat for the northern Gulf of Mexico (GOM). In September 2004, Hurricane Ivan removed a
5 large volume of sediment from the eastern ends of Horn and Petit Bois islands with its 1 to 2 m
6 storm surge and ~194 kph wind speeds. Then, in August 2005 Hurricane Katrina severely
7 impacted the two islands again with its 3.5 to 5.5 m storm surge on Horn and Petit Bois islands,
8 and estimated maximum sustained wind speeds of 204 kph at landfall in southeast Louisiana.
9 Using topographic light detection and ranging (LIDAR) datasets from 2004 to 2016, spatial and
10 temporal changes of the islands' area, sediment volumes, and shorelines were measured to
11 ascertain their geomorphic responses and recovery rates following the impacts of these devastating
12 tropical cyclones. During the 2004–05 hurricane seasons, Horn Island lost ~13.3% of its pre-
13 hurricane Ivan land area, lost ~35.9% sediment volume, and had a total average shoreline change
14 rate of –10 m/yr. Petit Bois Island also lost ~13.3% of its pre-Ivan land area, lost ~27% sediment
15 volume, and had a shoreline change rate of –33 m/yr. Between 2005 (post-Katrina) and 2016,
16 Horn Island recouped ~6.6% of its pre-Ivan land area and ~4.3% sediment volume, whereas Petit
17 Bois Island recovered ~4% of its pre-Ivan land area and ~22.9% sediment volume. The overall
18 averaged shoreline change rates between 2004 and 2016 were –2 m/yr for Horn Island and –3 m/yr
19 for Petit Bois Island. These changes reflect that Horn Island is no longer stable, as its sediment
20 supply cannot keep pace with the current rate of sediment loss, and that because Petit Bois Island's
21 narrow central shoreline is retreating at a rate of 10 m/yr, the island is at risk of breaching during
22 the next storm. Highlighting complex island response, the relationship between area and shoreline
23 changes to that of volume changes was inconsistent.

24 **KEYWORDS**

25 LIDAR; Barrier island geomorphology; Hurricanes; Sediment transport

26 **1. INTRODUCTION**

27 Barrier islands worldwide are increasingly at risk of being lost or deteriorated due to a
28 myriad of forcing mechanisms (Fearnley et al., 2009; Lentz and Hapke, 2011; Odezulu et al.,
29 2018). Accelerating rates of sea level rise (SLR) (Jevrejeva et al., 2014), increased tropical cyclone
30 frequency and intensity (Walsh et al., 2016), and variations in sediment supplies (Gabriel and
31 Kreutzwiser, 2000) have contributed to beach erosion, shoreline migrations, and/or submergence
32 of barrier islands in many coastal zones (Morton, 2008; Salzman et al., 2013; Rodriguez et al.,
33 2018). Additionally, the dredging of shipping channels for navigation and the installation of
34 artificial coastal structures around barrier islands have altered patterns of sediment delivery
35 (Edwards, 2006; Morton, 2008; Otvos and Carter, 2008; Byrnes et al., 2013).

36 Temporal and spatial distributions of barrier islands using two-dimensional (2D) datasets
37 have quantified area, width, and shoreline positions for decades (Waller and Malbrough, 1976;
38 Morton et al., 2004; Sciaudone et al., 2016) using various field, hydrographic, and remote-sensing
39 methods. Recently, the availability of high-resolution LIDAR data have expanded those analysis
40 capabilities into three-dimensions (3D), allowing for the quantification of elevation and/or
41 sediment volume on beaches and barrier islands worldwide, such as on the United States' East,
42 West, and Gulf coasts (Buijsman et al., 2003; Preistas and Fagherazzi, 2010; Lentz and Hapke,
43 2011; Conery et al., 2018), the northeast Canadian coast (Xhardé et al., 2011), and United
44 Kingdom coasts (Saye et al., 2005). While LIDAR data exist for a variety of coastal and nearshore
45 environments, few studies have conducted high-resolution difference analyses over large areas
46 (Buijsman et al., 2003; Zhang et al., 2005; Gares et al., 2006; Eisemann et al., 2018). By

47 quantifying centimeter to decimeter-scale vertical changes (NOAA, 2012) over large coastal
48 regions (10s of kilometers), barrier island response to sea level rise, storm impacts, and sediment
49 supply can be better understood over annual to decadal timescales. Additionally, these data can
50 be used to constrain barrier island evolutionary numerical models, such as XBEACH (Harter and
51 Figlus, 2017), BIT (Masetti et al., 2008), GEOMBEST (Moore et al., 2007), and BRIE (Nienhuis
52 and Lorenzo-Trueba, 2019).

53 In the United States, barrier island chains located along the northern GOM perimeter are
54 considered among the most vulnerable to erosion or submergence (Otvos and Carter, 2013;
55 Eisemann, 2016; Eisemann et al., 2018), due to a combination of the aforementioned
56 environmental and anthropogenic forces. Of particular concern to the northern GOM community
57 is the Mississippi-Alabama (MS-AL) barrier island chain. Previous work examining changes on
58 decadal to centennial scales concluded the MS-AL barrier islands have undergone long-term
59 shoreline erosion (Waller and Malbrough, 1976; Byrnes et al., 1991; Morton et al., 2004) and
60 significant land area reductions since the mid-1800's (Waller and Malbrough, 1976; Morton, 2008;
61 Otvos and Carter, 2013) primarily due to tropical cyclone impacts, sediment budget deficits, SLR,
62 and human activities (Waller and Malbrough, 1976; Morton, 2008; Otvos and Carter, 2008; Byrnes
63 et al., 2013). Of these forcing mechanisms, research has focused mainly on changes before and
64 after major storm events (Morton and Sallenger, 2003; Schmid, 2003; Froede, 2006; Fritz et al.,
65 2007; Morton, 2010; Jones, 2015). A shoreline change study by the United States Geological
66 Survey (USGS), using four historical shoreline positions and one LIDAR-derived modern
67 shoreline, determined the long-term (~150 yrs) shoreline change rate for Mississippi was -2.3 m/yr
68 (15 year, short-term rate of -2.1 m/yr), and for Alabama -0.4 m/yr (20 year, short-term rate $+0.3$
69 m/yr) (Morton et al., 2004). While this method of coastal monitoring provides quantitative

70 analyses of shoreline change in a 2D plane, it omits the spatial changes occurring on barrier
71 islands' interiors (e.g., dunes, ridges, swales, ponds and lagoons). By incorporating 3D barrier
72 island changes, highly dynamic spatial and temporal processes can be quantified. This study seeks
73 to extend the current state of knowledge of the MS barrier islands by quantifying area, volume,
74 and shoreline change on Horn and Petit Bois islands (Fig. 1).

75 **1.1 Regional Setting**

76 The MS-AL barrier island chain (Fig. 1) is a set of six offshore islands situated from 5 to
77 20 km seaward of the mainland coast. From west to east, the five main islands in the MS-AL
78 barrier island chain are Cat Island, Ship Island, Horn Island, and Petit Bois Island in Mississippi,
79 and Dauphin Island on Alabama's southwest coast. This approximately 100 km long assemblage
80 of islands and tidal passes form the geographical demarcation between the Mississippi Sound and
81 the northern GOM (Eleuterius, 1978). The islands are composed of 50 to 100% fine to pebble-
82 sized (0.21 to 4 mm) quartz sand (Waller and Malbrough, 1976; Cipriani and Stone, 2001), 2 to
83 50% heavy minerals (0.061 to 0.495 mm) (Foxworth et al., 1962; Cipriani and Stone, 2001), and
84 <2% calcium carbonate shells (Cipriani and Stone, 2001).

85 The initiation of the MS-AL barrier chain took place between 6 ka and 4 ka years BP
86 (Otvos, 2005; Hollis, 2018) when the western side of incipient Dauphin Island, anchored by the
87 Pleistocene Gulfport Formation towards the east (Otvos, 1985), intersected with landward
88 migrating marine shoals at an ~2 mm/yr SLR rate. As SLR decelerated below 2 mm/yr, the in-
89 situ shoals received enough sediment from alongshore and offshore sources to vertically aggrade
90 and stabilize (Otvos, 1979, 1981, 2018; Hollis, 2018; Hollis et al., 2019), forming modern day
91 Dauphin Island. Horn Island formed ~5 ka years BP at an ~1 mm/yr SLR rate (Otvos, 2005; Gal,
92 2018). Sand sourced primarily from the ravinement of the Biloxi and Pascagoula river

93 paleochannels south of Horn Island contributed considerably to its evolution (Gal, 2018). Ship
94 Island and the eastern part of Cat Island formed ~4.6 ka years BP as westward littoral transport
95 facilitated the vertical aggradation of Mississippi shoals over preexisting Holocene sandy-muds
96 (Otvos, 1985, 2001). The extent of westward progradation of the barrier islands ceased when it
97 encountered the advancing St. Bernard delta lobe of the southeast Louisiana coast, ~3.8 ka to 1.8
98 ka years BP (Twichell et al., 2013). Evidence of intense hurricanes impacting the northern GOM
99 have been geologically documented between ~2.2 to 1.9 ka and ~0.9 to 0.6 ka years BP by Bregy
100 et al. (2018), and modern day Petit Bois Island was given its own designation following a
101 hurricane-induced separation from Dauphin Island, likely in the mid-eighteenth century (Otvos,
102 1979). The sixth “island”, West Petit Bois Island (WPBI), originated as spoils of dredging
103 operations from the Pascagoula Shipping Channel between 1917 and 1920 (Byrnes et al., 2013).
104 In May 2018, WPBI was officially added to the National Park Service’s Gulf Island National
105 Seashore (Everitt, 2018), which previously included western Cat, Ship, Horn, and Petit Bois
106 islands.

107 The MS-AL barrier chain is set in a subtropical climate on a passive margin. Surface winds
108 are predominately from the east (E) and southeast (SE) between April and August, from the south
109 (S) in July, and from the E and northeast (NE) between September and March (Waller and
110 Malbrough, 1976; Byrnes et al., 1991; Zavala-Hidalgo et al., 2014). The islands are subject to
111 averaged significant wave heights of 0.4 to 0.7 m (Byrnes et al., 2013) and diurnal tides of 0.3 to
112 0.6 m (Waller and Malbrough, 1976).

113 Meteorological systems in this region strongly influence the geomorphology of the MS-
114 AL barrier islands. Under moderate conditions, the wave climate controls a net sediment flux of
115 230,000 – 305,000 m³/yr via littoral drift (Byrnes et al., 2013). However, during periods of severe

116 weather, increased water levels increase normal wave heights (Byrnes et al., 1991) causing dune
117 and shoreface erosion. Severe weather systems include tropical cyclones, extratropical cyclones,
118 and cold fronts. Of these three systems, tropical cyclones have been acknowledged to cause the
119 most discernible changes to the sediment budgets of the islands (Morton and Sallenger, 2003;
120 Otvos and Carter, 2008; Jones, 2015). This is because their high velocity, sustained surface winds
121 and gusts (>119 kph) (NOAA, 2012) initiate dune blowouts (Gabriel and Kreutzwiser, 2000), and
122 generate high energy waves and storm surges, leading to island fragmentation, island breaching,
123 overwash (Otvos and Carter, 2008; Morton, 2010), inundation (Sallenger, 2000; Fritz et al., 2007),
124 and/or saltwater flooding (Waller and Malbrough, 1976). The less severe, yet more frequently
125 occurring extratropical cyclones and cold fronts are accompanied with directional-shifting, mild
126 to moderate (with occasionally gusting) surface winds and lower-energy waves (Masselink and
127 van Heteren, 2014), which have been recognized as erosive (Keen, 2002), restorative (Chaney,
128 1999), or adjusting (Stone et al., 2004) forces to the barrier islands.

129 **1.2 Study Sites**

130 Horn Island (Fig. 2) is ~19.5 km long and is centrally located in the MS-AL barrier island
131 chain. Its orientation is largely shore-parallel with a southern, concave coastline near its center.
132 Horn Island was first identified as Mississippi's "most stable barrier island" by Byrnes et al. (1991)
133 due to its resiliency to tropical cyclone impacts, relative to the other islands. They determined that
134 from 1849 to 1986 Horn Island sustained no breaches or major shoreline alterations and had the
135 least cumulative percent change (15%) in its land area during that time (Byrnes et al., 1991). On
136 a short-term time scale, 1976 to 1986, Byrnes et al. (1991) found that Horn Island's rate of areal
137 change was -6.4 hectares/yr (or -0.064 km²/yr). These results were later corroborated in similar
138 studies by Morton (2008), showing a 19% land area change for the period of 1849 through 2007,

139 and a short-term change rate of -5.7 hectares/yr (or -0.057 km²/yr) between 1986 and 1998
140 (Morton, 2007). In a more recent study, Gal (2018) found that the continued stabilization of the
141 island is due to sand sourced from the ravinement of two incised valley paleochannels that
142 converge and intersect Horn Island.

143 Petit Bois Island (Fig. 2), situated between Horn and Dauphin islands, is ~ 10.4 km long
144 with a convex southern shoreline, and has a distinct triangular shape on its eastern half. A 1732
145 map of the north-central GOM coast by French cartographers Anville and Haye (1752) depicted
146 only four barrier islands fronting the MS Sound, indicating modern-day Petit Bois Island was once
147 part of Dauphin Island. Otvos (1979) suggests an unnamed hurricane, possibly in 1740, segmented
148 the island in two. Since then, Petit Bois Island has been migrating laterally to the west via updrift
149 erosion and downdrift accretion (Byrnes et al., 1991) between episodes of tropical cyclone
150 impacts. Its short-term areal change rates were found to be -2.8 hectares/yr (or -0.028 km²/yr)
151 between 1976 and 1986 (Byrnes et al., 1991) and -10.0 hectares/yr (or -0.1 km²/yr) between 1986
152 and 1998 (Morton, 2007). Petit Bois Island's western flank is currently abutting the Pascagoula
153 Shipping Channel, preventing its continued westward migration due to ongoing dredging
154 operations by the U.S. Army Corps of Engineers (Byrnes et al., 2013).

155 **1.3 Cyclone History**

156 During the study period (2004-2016), eight tropical cyclones passed within a 200 km radius
157 of Horn and Petit Bois islands (Table 1). Hurricane Cindy (2005), Hurricane Katrina (2005),
158 Tropical Storm Lee (2011), and Hurricane Isaac's (2012) storm tracks all passed to the west of the
159 islands, meaning they experienced the "right sides" of the tropical cyclones. In the northern
160 hemisphere, the right sides of tropical cyclones are where the strongest winds and storm surges are
161 produced (Landsea, 2014). In these instances, the islands would have been subjected to more

162 erosive forces than those storms passing to the islands' east (Fearnley et al., 2009), such as in the
163 cases of Hurricane Ivan (2004), Tropical Storm Arlene (2005), Hurricane Dennis (2005), and
164 Tropical Storm Ida (2009). Horn and Petit Bois islands' geomorphic responses to these tropical
165 cyclones and their post-storm periods have been digitally captured using LIDAR technology.

166 **1.4 Study Goals**

167 Previous studies on MS-AL barrier island evolution using various methods have
168 demonstrated long-term vulnerability (Waller and Malbrough, 1976; Byrnes et al., 1991, 2013;
169 Morton et al., 2004; Morton, 2008; Otvos and Carter, 2013; Eisemann et al., 2018). The unique
170 approach taken here is the use of multi-year, 3D, high-resolution LIDAR data to analyze the
171 geomorphic responses of the islands before and after tropical cyclone impacts, including periods
172 with no activity. This technique was first employed on Ship Island (Fig. 1) by Eisemann et al.
173 (2018), as no studies had quantified sediment volume changes in high-resolution on the MS-AL
174 barrier chain. The present study expands upon Eisemann et al.'s (2018) work by applying similar
175 LIDAR-based methods to Horn and Petit Bois islands to determine land area and volume
176 differences, and rates of shoreline change between 2004 and 2016. The goal of this study is to
177 compare the changes on Horn and Petit Bois with those of Ship, allowing us to better understand
178 the complex responses of these islands to variations in sediment supply, sea level rise, and storm
179 impacts. Specifically, what immediate geomorphic changes resulted from a hyperactive hurricane
180 season versus the following years when fair-weather conditions drove changes? This approach
181 provides insight into barrier island processes, such as overwash, dune accretion/erosion, and
182 shoreface erosion, rarely quantified, which will be of broad scientific interest. Additionally,
183 specific to LIDAR-derived geomorphic changes, are shoreline and areal changes always

184 proportional to volume changes for barrier islands? Answering this question is key to providing
185 general methodological approaches that will be internationally applicable.

186 Lessons learned from this study have global implications, as there is a dearth of high-
187 resolution, yet large spatial scale volumetric analyses for numerous barrier islands in a single
188 chain. Data derived from this study could be important input parameters for generalized barrier
189 island numerical modeling around the world.

190 **2. METHODS**

191 *2.1 LIDAR Acquisition and Digital Elevation Model Generation*

192 LIDAR datasets for Horn and Petit Bois islands were acquired from the National Oceanic
193 and Atmospheric Administration's (NOAA) Data Access Viewer for years 2004, 2005, 2007,
194 2011, and 2016 (Table 2). These 3D, high-resolution datasets provide continuous surfaces across
195 a wide geographic area, allowing for the differences in elevation, shoreline positions, sediment
196 volume, and area of the barrier island platforms to be calculated during the 12.5-year study period.
197 LIDAR data analyses were conducted for five periods: April 2004 – December 2005, December
198 2005 – June 2007, June 2007 – June 2011, June 2011 – October 2016, and the entire period from
199 April 2004 to October 2016. The first period (2004 – 2005) captured two cycles of the North
200 Atlantic hurricane seasons, which included three major (category 3 or higher) tropical cyclone
201 impacts to the northern GOM, whereas the following three periods had 0 to 2 tropical cyclones per
202 year (category 2 or lower) during the next 11 hurricane seasons. The final period, 2004 to 2016,
203 looks at the net differences from beginning to end. The data time series provided the opportunity
204 to determine the islands' geomorphic responses and recoveries to these meteorological events.

205 Topographic-bathymetric point data in XYZ (longitude, latitude, elevation) format were
206 provided referenced to the earth's bare surface (excluding vegetation or artificial structures), to the

207 NAD83 horizontal datum in decimal degrees, and to the NAVD88 vertical datum in meters (m).
208 A sample set of elevation points (Z-values) from the entire study area's four-corners were then
209 processed through NOAA's VDatum Transformation v3.6 tool to obtain an average conversion
210 offset value between the NAVD88 and local mean high water (MHW) datums. This offset (or
211 correction) value was then applied across the entire dataset, allowing for comparisons of elevation
212 and sediment volume changes to be more spatially accurate. The resulting MHW is $0.36 \text{ m} \pm 0.01$
213 m above NAVD88, therefore, subtracting 0.36 m from each terrain elevation point effectively
214 transformed the datasets from NAVD88 to local MHW (consistent with Eisemann et al., 2018).

215 Digital elevation models (DEMs) for each year (Fig. 3) were then generated using
216 MATLAB software gridded to $5 \times 5 \text{ m}^2$ cellular resolution (linear interpolation algorithm; from
217 Eisemann et al., 2018). Individual datasets were uniformly cropped to contain point data for each
218 barrier platform as a separate area of interest. The gridded cells were then tabulated to yield total
219 areas and volumes for each island per year. LIDAR survey coverages, however, of Horn and Petit
220 Bois islands were spatially variable in both topography and bathymetry. Only two of the five
221 datasets (2007 and 2016) contained nearshore bathymetry down to 14 m depth (relative to MHW),
222 whereas all five datasets contained topographic elevation of Horn and Petit Bois islands. Two
223 caveats with respect to the topographic elevation points are that: a.) the 2004 dataset excluded
224 $\sim 0.95 \text{ km}^2$ (satellite estimated area) of coverage from the northern-most side of Horn Island (Fig.
225 3, 2004, missing coverage) and $\sim 0.62 \text{ km}^2$ (satellite estimated area) of coverage from the northeast
226 side of Petit Bois Island, and b.) the 2005 dataset excluded $\sim 0.22 \text{ km}^2$ (satellite estimated area) of
227 coverage from the northeast side of Petit Bois Island during the flight surveys for those years. As
228 a result of these observations, all LIDAR-derived area values were cross-referenced to satellite
229 imagery to ensure subaerial LIDAR data points were captured for both islands.

230 **2.2 LIDAR Uncertainty**

231 Positional uncertainty is reported in the metadata accompanying each LIDAR dataset. The
232 reported maximum vertical uncertainty of all five datasets was 20 cm, and the maximum horizontal
233 uncertainty was 100 cm (Table 2). These uncertainty values are primarily associated with
234 collection errors in the onboard aircraft equipment, including the GPS, the inertial navigation unit,
235 and the unit that points the direction of the laser (Hodgson and Bresnahan, 2004; Lentz and Hapke,
236 2011). Quality control of post-processed LIDAR data can be assessed by calculating the horizontal
237 and vertical offsets between multiple datasets using a stationary structure within the confines of
238 the respective study area (Lentz and Hapke, 2011; Eisemann et al., 2018). The present study area
239 did not contain a permanent structure to apply this quality control assessment to, so using methods
240 from Eisemann et al. (2018), the five datasets were plotted over Fort Massachusetts on Ship Island,
241 and the vertical error was measured at ± 0.09 m (applied to all datasets). Horizontal uncertainty
242 was not a considerable factor relative to the large-scale changes identified in the results, as
243 confirmed by cross-validation with aerial satellite imagery.

244 **2.3 Subaerial Area Analyses**

245 To identify the total area and total areal changes in the subaerial landscape between two
246 DEMs, 2D surface contours of the islands' perimeters were generated using the 0 m MHW
247 elevations of each dataset. Once the 2D surfaces were created and gridded to 5 x 5 m² (25 m²)
248 cells, the summation of the cells produced the total area of each individual dataset. Subtracting an
249 older dataset from the subsequent, more recent dataset (for example, 2016 minus 2011) resulted in
250 the total areal changes between the two years. As previously mentioned, ~0.95 km² is missing
251 from Horn Island and ~0.62 km² is missing from Petit Bois Island's 2004 LIDAR surveys. Total
252 area calculations removed these missing sections for each subsequent year. Therefore, the total

253 areal change values between two subsequent datasets reflect these limitations and represent
254 minimum change values. Calculations were performed using MATLAB software.

255 **2.4 Volumetric Analyses**

256 DEM surfaces were directly analyzed using subtraction calculations (from Buijsman et al.,
257 2003 and Eisemann et al., 2018) to determine sediment volume gains and/or losses relative to the
258 local MHW datum. Elevation differences between overlapping datasets in coincident cell volumes
259 between time-1 (t_1) and time-2 (t_2) were calculated and output into new gridded surfaces to
260 spatially visualize where changes occurred on the islands. These differences in elevation (in
261 meters) were then multiplied by the area of each cell (25 m^2) to yield the volumetric changes in
262 cubic meters (m^3). Repeating this method on all datasets for topographic sediment volume
263 (ΔV_{topo}) (Eq. 1) and two datasets for bathymetric sediment volume (ΔV_{bathy}) (Eq. 2) allows us to
264 observe trends in sediment volume changes throughout the 12.5-year period. Where ΔV_{topo} and
265 ΔV_{bathy} returned positive values, sediment accreted, and where ΔV_{topo} and ΔV_{bathy} returned
266 negative values, sediment eroded (consistent with Eisemann et al., 2018):

$$267 \quad \Delta V_{topo} = V_{t_2} - V_{t_1} \quad (1)$$

$$268 \quad \Delta V_{bathy} = -(V_{t_2} - V_{t_1}) \quad (2)$$

269 Difference grids were created from one year relative to the previous year but are solely for
270 visualization purposes and are not used for volume change analyses. On account of the 2004
271 dataset having the geographically smallest area for topography, total subaerial volume calculations
272 for all individual datasets were adjusted to the greatest common areas of Horn and Petit Bois
273 islands' 2004 dataset, delineated by the pink dashed perimeter in Figure 3. Therefore, total
274 subaerial volume change values between two subsequent datasets reflect these limitations and
275 represent minimum change values. Additionally, because the 2007 dataset was the geographically

276 limiting dataset for bathymetry, the total bathymetric sediment volume and their differences
277 between 2016 and 2007 are limited to this area.

278 **2.5 Transect Elevation Profiles**

279 Elevation profile bundles were created from transects taken on Horn and Petit Bois islands
280 by subsampling LIDAR elevation data along those transects. One east and three south trending
281 transects on each island were selected to capture the largest geomorphic variabilities in topography
282 and bathymetry. Individual dataset profiles were plotted along these transect lines from 3D point
283 data using a linear interpolation algorithm (Buijsman et al., 2003), however, bathymetry was
284 limited to the 2007 and 2016 datasets.

285 **2.6 Shoreline Analyses**

286 The ArcGIS v10.5 software package and the USGS's Digital Shoreline Analysis System
287 (DSAS) v4.3 tool (Thieler et al., 2009) were used to quantify the 12.5-year shoreline change rates
288 on Horn and Petit Bois islands. The 2D DEMs were imported as XYZ files into ArcMap, and the
289 0 m MHW shorelines were reproduced and projected to the WGS84 UTM Zone 16 North
290 horizontal datum. The DSAS tool was then used to create bulk cross-shore transects spaced at 25
291 m intervals perpendicular to Horn and Petit Bois islands. This resulted in ~1200 transects for Horn
292 Island and ~610 transects for Petit Bois Island which were used to calculate end point rate statistics.
293 The statistical results yielded average annual rates of shoreline change, reported in meters per year
294 (m/yr). Finally, a visual inspection was conducted on questionable transects (i.e., those cutting
295 through broken/fragmented shorelines) to remove any potentially anomalous data, and cross-
296 checks were made to satellite imagery to confirm shoreline positions and geomorphic features.
297 Zero-meter shoreline contours were all adjusted to the 2004 dataset for Horn and Petit Bois islands,
298 so the total average shoreline change rates are considered minimum change values.

299 **2.7 Wave and Wind Data Analyses**

300 To understand the dynamics of physical forces and the effects they have on the islands'
301 geomorphologies, historical wave and wind data were obtained from several offshore buoys near
302 Horn and Petit Bois islands. First, significant wave height data were extracted from two moored
303 National Data Buoy Center (NDBC) buoy datasets and one University of Southern Mississippi
304 buoy (via Bender et al., 2010) to time-average wave energy calculations. Station 42007, situated
305 ~17 km south of Horn Island, provided one data-point per hour for each 24-hour period from
306 January 2004 to December 2009 (NDBC, 2018). Station 42012-Orange Beach, ~23 km southeast
307 of Petit Bois Island, provided one data-point per hour for each 24-hour period from April 2009 to
308 December 2016 (NDBC, 2018). Station 42067-USM3M01's (~20 km south of Horn Island)
309 significant wave height data were obtained from Bender et al. (2010). Using significant wave
310 heights and Holthuijsen's (2007) random-phase/amplitude model, wave energy (E) was calculated
311 using

$$312 \quad E = \rho g \left(\frac{1}{16}\right) (H_{m_0})^2, \quad (3)$$

313 where ρ is the density of seawater (1029 kg/m³), g is the acceleration due to gravity (9.81 m/s²),
314 and H_{m_0} is significant wave height (m). This equation produces units of wave energy per area in
315 Joules per meter squared (J/m²). Wave energy was then time-averaged over 24-hour periods for
316 the entire study period and used in conjunction with wind data to assess geomorphic changes.

317 Next, historical wind speeds and wind directions were extracted from two NDBC buoy
318 datasets to create wind-rose diagrams using the 'WindRose.m' v1.3.1.0 MATLAB function
319 (Pereira-Valadés, 2015). Hourly averaged wind data from January 2004 to December 2008 were
320 used from station 42007, and from January 2009 to December 2016 data were used from station
321 PTBM6, located approximately 0.25 km southwest of Petit Bois Island (NDBC, 2018). The wind-

322 rose diagrams portray graphical representations of wind speeds, directions, and directional
323 frequencies (or magnitudes) from January 2004 – December 2016.

324 Wave and wind periods were selected to be slightly longer than the LIDAR dataset periods
325 in order to capture the meteorological and oceanographic trends driving the geomorphic changes
326 on the islands. For these two parameters, period 1 (P1) is from January 2004 to December 2005,
327 period 2 (P2) is from January 2006 to July 2007, period 3 (P3) is from August 2007 to June 2011,
328 period 4 (P4) is from July 2011 to December 2016, and period 5 (P5) is from January 2004 to
329 December 2016 (Table 3). These data were used to determine direction and magnitude of wind
330 waves approaching the islands, and for determining storm activity which impacted the islands.

331 **3. RESULTS**

332 **3.1 Wave and Wind Data**

333 Wave energy as a function of time is plotted in Figure 4. Each line represents a 24-hour
334 mean energy, with maximum energies all corresponding to tropical cyclone impacts. Hurricane
335 Katrina produced the highest average (26.6 kJ/m^2) (Bender et al., 2010), followed by hurricanes
336 Gustav (15.8 kJ/m^2), Ivan (13 kJ/m^2), Isaac (11.2 kJ/m^2), Ike (10 kJ/m^2), and tropical storm Ida (8
337 kJ/m^2). Hurricane Katrina's landfall in August 2005 generated the largest (43.5 kJ/m^2) single value
338 (Bender et al., 2010) for the study period. Although hurricanes Gustav and Ike's storm tracks fell
339 outside of the designated 200 km radius (gray circle in Fig. 4), their storm surges and wave energies
340 were large enough to cause erosion to the low-elevated portions of the islands. The mean wave
341 energy for this study was $0.423 \pm 0.80 \text{ kJ/m}^2$. Statistical summaries of wave data are in Table 3.

342 Figure 5a is a wind-rose diagram depicting the distributions of wind speeds, wind
343 directions, and their magnitudes, for 2004 to 2016. The wind-rose indicates the dominant direction
344 for the study period was from the SE, meaning that for 8.1% of the time (or 11.2 months of

345 available data) prevailing winds were from the SE. Using a modified Beaufort Wind Scale (Storm
346 Prediction Center, n.d.), this wind rose diagram also illustrates that moderate winds (4.0 to 7.9
347 m/s) were present for 50.6% of the time (70.3 months), gentle winds (0 to 3.9 m/s) were present
348 for 34.1% of the time (47.3 months), strong winds (8.0 to 11.9 m/s) were present for 13.9% of the
349 time (19.3 months), and gale to storm force winds (≥ 12 m/s) were present for 1.3% of the time
350 (1.9 months). The 24-hour mean wind speed for this study was 5.33 ± 2.6 m/s and the maximum
351 (10-minute mean) wind speed was 34.4 m/s from the S-SE (Howden et al., 2008) during Hurricane
352 Katrina.

353 Figure 5b is a wind-rose diagram for July 2011 to December 2016. During this time, the
354 dominant wind direction was from the ENE, inconsistent with trends analyzed from all other
355 periods. The cause of this anomalous shift in wind direction was likely due to a low number of
356 tropical cyclones and an increased number of cold fronts passing through the area, relative to other
357 periods. Following the passage of a cold front, postfrontal, northerly winds transport sand from
358 both the mainland coastline and the north sides of Horn and Petit Bois islands towards the south,
359 which results in deposition along the southern foredunes and beaches. Thomason (2016) reported
360 that 205 cold fronts passed through coastal Louisiana and Mississippi from January 2011 to March
361 2016, and Iowa State University's Environmental Mesonet recorded ~35 more passed through the
362 end of 2016.

363 **3.2 Horn Island**

364 Figure 6 is a transect map of one east trending and three south trending transect lines cast
365 through Horn Island. LIDAR-derived elevation profiles for each year were plotted along the
366 transects to identify internal changes on the island. Cross-shore transects through Horn Island
367 were selected to approximately quadrisection the island.

368 **3.2.1 Elevation Transect Data**

369 **3.2.1.1 Transect H1**

370 Transect H1 (Fig. 7) is located on the western half of Horn Island. In the 2004 elevation
371 profile, the northern half of the island is generally <1 m, except for a few ~1.5 m backbarrier dunes,
372 and the southern half of the elevation profile is between 1 and 2.3 m, including one foredune and
373 two secondary dunes. The 2005 profile shows reduced surface elevations to all these dunes, with
374 the largest reduction to the southern foredune. On the 2007 profile, vertical elevation gains as
375 much as 0.5 m above the 2005 profile can be observed on the interior of the transect, whereas no
376 gains were observed on the shorelines. Bathymetry of the 2007 profile exhibits a steep upper
377 foreshore slope on the south-side down to -3 m, and a steep slope down to -2 m on the north-side.
378 The 2011 profile indicates dune scarping and vertical accretion on both north and south facing
379 dune ridges. The 2016 profile shows elevation increases of at least ~0.5 m across the entire length
380 of the transect, including shoaling in the bathymetry.

381 **3.2.1.2 Transect H2**

382 Transect H2 (Fig. 8) is positioned through central Horn Island. The 2004 profile shows
383 the greatest variability in topographic elevations, including dune ridges between 2.5 and 3.6 m.
384 The profiles for 2005, 2007, and 2011 indicate erosional trends in relation to storms. The exception
385 is the northern and southern dunes, where elevation gains are observed from 2007 to 2016. The
386 2016 topographic profile is generally accretional, and elevations gains of 0.2 to 0.7 m over the
387 2011 profile can be observed. Bathymetric profiles from 2007 to 2016 show that erosion occurred
388 on the north side of the transect, whereas accretion occurred on the south side.

389 **3.2.1.3 Transect H3**

390 Transect H3 (Fig. 9) is located on the eastern half of Horn Island. In 2004, the highest
391 elevation points along this transect (from north to south) were a 4.6 m backbarrier dune and a 2.8
392 m interior dune, with a shallow lagoon situated just below MHW between the two; and, two
393 additional interior ridges between 2 and 2.3 m high. By 2005, the elevation profile shows the
394 backbarrier dune eroded by 0.3 m, while the interior dune flanking the lagoon eroded by 2.5 m,
395 and the two interior ridges eroded as much as 1 m. There was, however, ~1 m of sediment
396 accretion between kilometers 0.5 and 0.6 in the cross-shore direction between 2004 and 2005. The
397 2007 profile is generally accretional along the entire transect, except for the lagoon which
398 exhibited deepening. The 2011 profile shows a taller and narrower backbarrier dune, a reduction
399 in elevation in the center of the transect, and a vertically accreted foredune ~3 m in elevation. The
400 2016 elevation profile generally trends positive over 2011 across the majority of the transect,
401 including a final backbarrier dune height of 4.4 m. The foredune, however, that was present in the
402 2011 profile had eroded down to between 1.6 and 2 m in height by 2016.

403 **3.2.1.4** *Transect H4*

404 Transect H4 (Fig. 10) is a centrally positioned, east trending transect along the island
405 indicating maximum elevations existed in 2004. Elevation profiles for 2005, 2007, and 2011 are
406 all largely erosional. Specifically, peaks in the central 2005 profile, between along-shore distances
407 of 8 and 11 km, continued to erode between the 2007 and 2011 profiles. The 2016 elevation profile
408 was almost entirely accretional over the 2011 profile. Several of the 2016 dunes between
409 kilometers 12 and 13 in the along-shore distance even reached or exceed the 2004 elevations.

410 **3.2.2** *Subaerial Area and Shoreline Changes*

411 Area and shoreline (Table 4) changes between 2004 and 2016 were quantified for Horn
412 Island using differences in the 0 m MWH elevation points. Horn Island had a subaerial area of

413 13.43 km² in April 2004, which decreased to 11.64 km² by December 2005. During this time, the
414 eastern tip lost 0.31 km² and the western tip lost 0.17 km², contributing to a total average shoreline
415 change rate of -10 m/yr. From late 2005 to June 2007, the island's area increased to 12.34 km².
416 This increase was primarily due to spit progradation on the tips, and the re-emergence of 0.04 km²
417 of the 2004 far eastern tip, resulting in a total average shoreline change rate of +4.2 m/yr. From
418 mid-2007 to June 2011, Horn Island slightly reduced to 12.25 km² when the remnant tip
419 resubmerged, causing a total average shoreline change rate of -1.9 m/yr. Beyond 2011, Horn
420 Island's area continued to expand via spit progradation and lagoonal infilling to reach 12.52 km²
421 by October 2016, yet had a negative total average shoreline change rate of -0.8 m/yr. The reason
422 for this apparent conflict is because the shorelines of the interior lagoons were not considered in
423 the DSAS calculations (only peripheral shorelines were), but the overall area of the island was
424 accounted for within MATLAB. The overall net changes to Horn Island between 2004 and 2016
425 indicate that the subaerial area had decreased by at least 0.91 km², and the total average shoreline
426 change rate was -2 m/yr.

427 **3.2.3 Volume Changes**

428 Subaerial elevation differences between 2004 and 2016 were quantified from points above
429 MHW and are reported as changes in sediment volume. In April 2004, Horn Island contained
430 1.695×10^7 m³ of sediment and by December 2005 contained 1.086×10^7 m³. Horn lost 6.09×10^6
431 m³ (Table 5) of its volume due to erosion on the eastern and western tips, along with interior
432 surface erosion as much as -4 m (Fig 11a). Between late 2005 and June 2007 (Fig. 11b), minor
433 sediment gains occurred on the island's tips and southern foreshore; however, continued erosion
434 of the interior dune fields contributed to the further loss of 0.76×10^6 m³ of sand. From mid-2007
435 to June 2011, elevation gains between 0.5 and 2 m were observed on Horn's western tip, parts of

436 the southern foreshore, and several interior lagoons (Fig. 11c), yet the island lost another 1.05×10^6
437 m^3 sediment. From mid-2011 to October 2016, sediment volume on Horn increased by 2.54×10^6
438 m^3 to a final volume of $1.159 \times 10^7 \text{ m}^3$. Sediment gains were mainly accumulated across the
439 island's southern shore-parallel dune ridges, and interior lagoons (Fig. 11d). The net volumetric
440 change (Fig. 11e) to Horn Island between 2004 and 2016 was a minimum of $-5.36 \times 10^6 \text{ m}^3$. A
441 summary of Horn's subaerial area and volume quantities for the five datasets are graphically
442 represented in Figure 12.

443 Bathymetric elevation differences were quantified from points below MHW, to a
444 maximum depth of -4 m (Fig. 13) and are reported as changes in sediment volume. In 2007, the
445 nearshore water volume around Horn Island was $9.065 \times 10^6 \text{ m}^3$ (Table 6), which increased to
446 $9.462 \times 10^6 \text{ m}^3$ in 2016. Erosion as much as 4 m took place largely on the southeastern shoreface,
447 creating accommodation for a larger volume of water in this vicinity. On the northern side of the
448 island, sediment deposition as much as 1 m occurred in the nearshore. The overall bathymetric
449 sediment volume change for Horn Island between 2007 and 2016 was $-3.97 \times 10^5 \text{ m}^3$, indicating
450 an overall deepening.

451 **3.3** *Petit Bois Island*

452 Figure 14 is a transect map of one east trending and three south trending transect lines cast
453 through Petit Bois Island. LIDAR-derived elevation profiles for each year were plotted along the
454 transects to identify internal changes on the island. Cross-shore transects through Petit Bois Island
455 were selected to capture a tidal channel (PB1), the narrowest width (PB2) and the widest width
456 (PB3) of the island.

457 **3.3.1** *Elevation Transect Data*

458 **3.3.1.1** *Transect PBI*

459 Transect PB1 (Fig. 15) is located on the western end of Petit Bois Island. Shoreline
460 movement at the MHW line was minimal on either side of the island between 2004 and 2016.
461 Ridge and swale topography dominated this part of the island in 2004, and the two highest peaks
462 along this transect were 2.7 and 3 m in elevation. The 2005 elevation profile shows the southern
463 berm had been reduced by 0.25 m, the northern berm reduced by 0.7 m, and incisions made to the
464 tidal channel in the cross-shore direction between kilometers 0.2 and 0.3. The 2007 profile is
465 accretional on both sides of the channel yet becomes erosional toward the south. The 2011 profile
466 is generally accretional with elevation gains in several of the dunes, yet the southern berm retreated
467 ~21 m from 2007. The 2016 profile also displayed vertical gains across the entire transect, with
468 respect to both topographic and bathymetric elevations.

469 **3.3.1.2** *Transect PB2*

470 Transect PB2 (Fig. 16) is centrally located on Petit Bois Island. Evidence of island
471 narrowing on the south-side, and sediment redistribution to the north-side is visible in this set of
472 profiles. In 2004, the width of the subaerially exposed land mass along this transect was 373.4 m,
473 the southern foredune ridge was 1.6 m high by 90 m wide, and the back half of the island was
474 almost entirely <1 m in elevation. By 2005, the foredune was reduced to 1.4 m high by 167 m
475 wide. In the subsequent profiles, the foredune began to vertically accrete and narrow, so that by
476 2016 it measured 2.5 m high by 49 m wide. The southern shoreline retreated 117 m between 2004
477 and 2016, with the largest retreat taking place between 2011 and 2016; and the northern shoreline
478 retreated 13.5 m between 2004 and 2016. Thus, the width of the subaerially exposed landmass in
479 2016 was 242.9 m. Bathymetry changes between 2007 and 2016 indicate the northern side of the
480 island vertically accreted by ~1 m, whereas the south side lost an average of 2 m.

481 **3.3.1.3** *Transect PB3*

482 Transect PB3 (Fig. 17) is located through the eastern portion of Petit Bois Island, capturing
483 it widest backbarrier. The 2004 profile is limited to the southern half of the island along this
484 transect. It shows several peaks no higher than 2.2 m. The 2005 profile, limited to the southern
485 two-thirds of the transect, is erosional and indicates ~40 m of shoreline retreat occurred on the
486 south-side. The 2007 elevation profile shows erosion to the southern foredune, then the profile
487 becomes accretional towards the north. The 2011 and 2016 profiles also indicate accretion. The
488 most notable features are the buildup of the backbarrier dune from 2007 to 2016, foredune
489 scarping, and shoreline erosion on the south side. Bathymetry profiles from 2007 to 2016 show
490 erosion occurred on the southern shoreface, while accretion occurred on the northern tidal flat of
491 the MS Sound.

492 **3.3.1.4** *Transect PB4*

493 Transect PB4 (Fig. 18) is a centrally positioned, east trending transect indicating the
494 greatest topographic variability was in 2004. Elevation profiles for 2005, 2007, and 2011 are all
495 erosional with the largest loss occurring between along-shore distances 3 and 4 km. The exception
496 being between the along-shore distances of 6 and 7 km, where accretion is observed. The 2016
497 elevation profile for Petit Bois Island was nearly entirely accretional. The most notable feature
498 along this transect is the western-most dune, which grew to 4.9 m by 2016, after losing 1.3 m
499 between 2004 and 2005.

500 **3.3.2** *Subaerial Area and Shoreline Changes*

501 Petit Bois Island's subaerial area was 4.00 km² in April 2004, which decreased to 3.47 km²
502 by December 2005. During this time, the eastern tip lost ~0.07 km² and the shoreline retreated as
503 much as 90 m, causing the island to narrow, and yielding a total average shoreline change rate of
504 -33 m/yr (Table 7). From late 2005 to June 2007, expansion of the eastern and western tips

505 increased the island's area to 3.74 km², resulting in a total average shoreline change rate of +5.2
506 m/yr. Between 2007 and 2011, Petit Bois Island's southeastern shoreline retreated between 35
507 and 50 m, and the area decreased to 3.64 km², producing a total average shoreline change rate of
508 -2.7 m/yr. By 2016, the southeastern shoreline continued to show evidence of retreat (Figs. 16
509 and 17), whereas the southwest shoreline advanced between 25 and 40 m. As a result, the island's
510 area slightly decreased to 3.63 km² and the total average shoreline change rate was -1.5 m/yr from
511 2011 to 2016. Overall, the net changes to Petit Bois Island between 2004 and 2016 indicate the
512 subaerial area had decreased at least 0.37 km² and the total average shoreline change rate was -3.1
513 m/yr.

514 **3.3.3 Volume Changes**

515 Petit Bois Island had 3.778 x 10⁶ m³ of sediment volume in April 2004 and 2.757 x 10⁶ m³
516 by December 2005 (Table 8). The loss of 1.021 x 10⁶ m³ between these years resulted from erosion
517 on the southern facing foredunes, eastern tip, and back barrier dunes. During this time, sediment
518 buildup on the interior dunes (Fig. 19a) occurred as a direct result of overwash from Hurricane
519 Katrina's storm surge. From late 2005 to June 2007, recovery began on the southern foreshore,
520 southeast tip, and western backbarrier tidal flats, while the central and western interior dune fields
521 underwent minor erosion, leading to a volume change of +1.34 x 10⁵ m³ (Fig. 19b). Between mid-
522 2007 and July 2011, the volume increased by only 0.68 x 10⁵ m³, mainly on the southeast foredune
523 (Fig. 19c). The largest accumulation of sediment to the island occurred between mid-2011 and
524 October 2016, when it gained 6.65 x 10⁵ m³ (Fig. 19d). Sediment accretion along the shore-parallel
525 southern dune ridges were due to the passages of cold fronts during this time. Despite these gains,
526 erosion to the south-central shoreface decreased the width of the narrowest part of the island.
527 Overall, the net subaerial volumetric change (Fig. 19e) on Petit Bois Island between 2004 and

528 2016 was a minimum of $-1.54 \times 10^5 \text{ m}^3$. A summary of Petit Bois Island's subaerial area and
529 volume quantities for the five datasets are graphically represented in Figure 20.

530 Table 9 shows the nearshore water volume around Petit Bois Island was $9.236 \times 10^6 \text{ m}^3$ in
531 2007, then decreased to $8.072 \times 10^6 \text{ m}^3$ in 2016. On the north side of the island, accretion up to a
532 maximum of +1 m (Fig. 21) was documented on the nearshore seafloor, reducing accommodation
533 for water volume in these areas. Shoreface erosion (as much as -4 m) was greatest on the southeast
534 and central parts of the island. In contrast, Petit Bois Island incurred the largest sediment gains
535 (as much as +4 m) to the shoreface in between these two erosional spots. The overall bathymetric
536 sediment volume change for Petit Bois between 2007 and 2016 was $+1.164 \times 10^6 \text{ m}^3$, indicating
537 shallowing.

538 4. DISCUSSION

539 4.1 Morphological Impacts / Responses of the 2004-2005 Hurricane Seasons

540 The 2004 and 2005 hurricane seasons produced three category 3 hurricanes which
541 impacted the northern GOM within 200 km of the study area. First, Hurricane Ivan passed 54 km
542 east of Petit Bois Island in September 2004, generating local storm surge heights of 1-2 m (Stewart,
543 2004), wave energy of 13 kJ/m^2 , and maximum 2-hr sustained wind speeds of 25.2 m/s (90.7 kph).
544 In July 2005, Hurricane Dennis passed 132 km east Petit Bois Island with a storm surge height of
545 0.8 m (Bevan, 2005), wave energy of 4.9 kJ/m^2 , and maximum 4-hour averaged wind speeds of
546 16.6 m/s (59.8 kph). Seven weeks later, at the end of August 2005, Hurricane Katrina made
547 landfall 100 km to the west of Horn Island with storm surge heights of 3.5 to 5.5 m (Fritz et al.,
548 2007), wave energy of 26.6 kJ/m^2 (Bender et al., 2010), and maximum 10-min averaged wind
549 speeds of 34.4 m/s (123.8 kph) (Howden et al., 2008) near Horn and Petit Bois islands.

550 The hurricanes' extreme atmospheric and oceanographic forces produced within a 12-
551 month period collectively caused numerous geomorphic changes to Horn and Petit Bois islands.
552 On Horn Island, the most obvious change was the loss of $\sim 0.4 \text{ km}^2$ of the eastern tip, accounting
553 for $1.54 \times 10^5 \text{ m}^3$ of sand between April 2004 and September 2005 (Fig. 22). The loss of this tip
554 was initiated with a breach during Hurricane Ivan from the 1 to 2 m storm surge to the low-lying
555 (0.5-1 m) sandbar. The breach was widened via erosion during Hurricane Dennis, and finally
556 completely submerged by Hurricane Katrina's storm surge. The western tip of Horn Island,
557 however, lost half as much land area ($\sim 0.2 \text{ km}^2$), yet $\sim 100,000 \text{ m}^3$ more sand (total $2.49 \times 10^5 \text{ m}^3$)
558 during Hurricane Katrina alone. Additional topographic changes between 2004 and 2005 included
559 dune lowering and flattening (2004 & 2005 profiles in transects H1-H3, Figs. 7-9), shoreface
560 erosion (Fig. 11a), washover deposits, and the loss of vegetation density (Carter et al., 2018) due
561 to saltwater inundation and burn. Therefore, as a result of these three storms, Horn Island had a
562 subaerial areal change rate of $-1.07 \text{ km}^2/\text{yr}$, a subaerial volume change rate of $-3.65 \times 10^6 \text{ m}^3/\text{yr}$,
563 and a shoreline change rate of $-10 \text{ m}/\text{yr}$ between 2004 and 2005.

564 Petit Bois Island was also negatively affected during the 2004 and 2005 hurricane seasons.
565 Similar to Horn Island, both hurricanes Ivan and Dennis caused erosion to the eastern tip of Petit
566 Bois, yet Hurricane Katrina produced the greatest geomorphic changes to the whole island. Figure
567 23 shows a zoomed in view of erosion to Petit Bois' southwestern foredune, illustrating where
568 $\sim 4,600 \text{ m}^3$ of sand (source sediment) was overwashed by Katrina's storm surge, and where $\sim 2,650$
569 m^3 of that sediment was deposited. The penetration distance of the overwashed sand was 217 to
570 240 m from the source. During this period, Petit Bois Island's southeastern foredunes were eroded
571 as much as 1.5 m in elevation, whereas the southwestern foredunes eroded as much as 4 m (Fig.
572 19a). Additionally, erosion along a low-lying tidal channel (Fig. 15; between kilometers 0.2 and

573 0.3 in the cross-shore distance) was initiated between 2004 and 2005 which lasted for the following
574 six years. Storm surge inundation also caused a 37% reduction in vegetation density across the
575 island (Carter et al., 2018). The geomorphic alterations between 2004 and 2005 caused Petit Bois
576 Island to incur a subaerial areal change rate of $-0.32 \text{ km}^2/\text{yr}$, a subaerial volume change rate of $-$
577 $6.13 \times 10^5 \text{ m}^3/\text{yr}$, and an average shoreline change rate of -33 m/yr .

578 **4.2 Morphological Responses from 2005 to 2016**

579 In the absence of intense, large-scale, tropical cyclones in the study area for the following
580 eleven hurricane seasons, the local fair-weather wave and wind climates became the dominant
581 forces driving sediment transport and morphological changes on the islands. Average significant
582 wave height from 2005 to 2016 was 0.65 m, average wave energy was $0.421 \pm 0.65 \text{ kJ/m}^2$, and the
583 prevailing wind-wave direction was from the SE. Since, wind facilitates aeolian transport of sand
584 grains on barrier beaches and dunes through saltation and creep (Bagnold, 1941), grain sizes of
585 0.25 mm on Horn and Petit Bois islands are capable of being moved and/or transported at minimum
586 speeds of 4.1 m/s, measured 1 cm above the surface (calculated using Bagnold's, 1941 equations).
587 Winds near Horn and Petit Bois islands $\geq 4 \text{ m/s}$ were present for 61% of the time, yielding favorable
588 conditions for aeolian sediment erosion or re-distribution. Wind speeds and directions also impact
589 wave dynamics in the area, such that wind generates surface waves and influences their direction
590 of travel (Thomason, 2016). The prevailing SE, moderate winds for the majority of the 12.5-year
591 study period (consistent with Zavala-Hidalgo et al., 2014) created a westward direction of sediment
592 transport (Byrnes et al., 2013). Strong to gale force winds, however, blew from the north ~17%
593 of the time which caused sediment from the back side of the islands to redistribute to the interior,
594 or transported sediment of the southern foredunes offshore.

595 **4.2.1 2005 (Post-Katrina) to 2007**

596 Between 2005 and 2007, Horn and Petit Bois islands entered a post-storm phase. During
597 this period, the islands experienced deposition in the form of spit growth on the eastern and western
598 tips (Figs. 11b and 19b), sediment accretion on their southern foreshores and beaches, a resurfaced
599 segment of the far-eastern 2004 tip of Horn Island (Fig. 11b), and the formation of a new lagoonal
600 perimeter on Petit Bois Island's northeastern side (Fig. 19b). Deposition on the islands' southern
601 shorelines were carried from the east, and though this period had the lowest average wave energy
602 ($0.342 \pm 0.48 \text{ kJ/m}^2$), the islands experienced their greatest shoreline expansions. Erosion of the
603 islands' interior dune ridges resulted from the lack of substantial vegetation necessary to retain
604 sediment in place (Carter et al., 2018). As a result, wind erosion of 2 to 3 m in elevation on Horn
605 and 0.5 to 1 m in elevation on Petit Bois occurred on the central part of the islands, as winds blew
606 dominantly from the E-SE. This resulted in deposition in several lagoons and ponds thereby
607 reducing their open water area. The depositional and erosional processes between 2005 and 2007
608 led to a subaerial areal change rate of $+0.44 \text{ km}^2/\text{yr}$, a subaerial volume change rate of -4.8×10^5
609 m^3/yr , and a shoreline change rate of $+4.2 \text{ m}/\text{yr}$ for Horn Island; and, for Petit Bois Island a $+0.17$
610 km^2/yr subaerial areal change rate, a $+8.46 \times 10^4 \text{ m}^3/\text{yr}$ subaerial volume change rate, and a $+5.2$
611 m/yr shoreline change rate.

612 **4.2.2 2007 to 2011**

613 The following period, 2007 to 2011, was climatically similar to the previous, with regards
614 to wave energy and prevailing wind direction, and the islands experienced relatively minor
615 geomorphic changes. Doran et al. (2009) reported that after Hurricane Gustav the dune elevation
616 changes on Mississippi's barrier islands were near 0 m, central Horn Island gained $\sim 100 \text{ m}$ of
617 shoreline, and Petit Bios Island lost $\sim 50 \text{ m}$ of shoreline at its center. LANDSAT imagery from
618 August to September 2008 revealed the combined effects of hurricanes Gustav and Ike did cause

619 erosion to the eastern ends of Horn and Petit Bois, but both islands showed signs of areal recovery
620 by February 2009; therefore, erosion caused by these storms was not evident in the LIDAR dataset
621 of 2011. In general, Horn Island's interior continued to erode during this period, while the tips
622 continued to add sediment and recover from the 2004-05 hurricane seasons. Petit Bois Island also
623 accumulated $\sim 7.7 \times 10^4 \text{ m}^3$ of sediment to its eastern tip's low-lying platform and backshore, and
624 $\sim 6.7 \times 10^4 \text{ m}^3$ of sediment on a small section of the southwestern berm (Fig. 19c). The southern
625 shoreline, however retreated between 20 and 40 m (Figs. 16 and 17), causing this side of the island
626 to narrow. The depositional and erosional processes from 2007 to 2011 led to a subaerial areal
627 change rate of $-0.02 \text{ km}^2/\text{yr}$, a subaerial volume change rate of $-2.68 \times 10^5 \text{ m}^3/\text{yr}$, and a shoreline
628 change rate of $-1.9 \text{ m}/\text{yr}$ on Horn Island; and, on Petit Bois Island a subaerial areal change rate of
629 $-0.03 \text{ km}^2/\text{yr}$, a subaerial volume change rate of $+1.74 \times 10^4 \text{ m}^3/\text{yr}$, and a shoreline change rate of
630 $-2.7 \text{ m}/\text{yr}$.

631 **4.2.3 2011 to 2016**

632 During the period of 2011 to 2016, Horn Island accumulated $2.54 \times 10^6 \text{ m}^3$ of sediment and
633 Petit Bois Island accumulated $6.65 \times 10^5 \text{ m}^3$, their largest quantities of sediment volumes (Tables
634 5 and 8) following the 2004-05 hurricane seasons. Notable areas of geomorphic change on Horn
635 and Petit Bois islands were to their southwestern foredunes and interior eastern halves (Figs 11d
636 and 19d), where Horn gained $\sim 6.5 \times 10^5 \text{ m}^3$ of sediment in these areas and Petit Bois gained ~ 2.8
637 $\times 10^5 \text{ m}^3$. Specific changes to the islands included dune building and lagoon in-filling (example in
638 Fig. 24) on both islands, erosion to the south-central shoreline of Horn Island, and an $\sim 60 \text{ m}$ retreat
639 (transect P2, Fig. 16) on Petit Bois Island's south-central shoreline. Changes during this period
640 may be explained by a variance in climatic conditions, likely resulting from an increased number
641 of cold fronts (Thomason, 2016) which moved into the study area from the north, relative to the

642 low number of tropical cyclones (Table 1). The wind-rose in Figure 5b shows the direction of
643 prevailing winds for this period were largely out of the ENE, an irregularity from the expected SE.
644 Winds from the northerly directions are responsible for relocating sediment from the north side of
645 the island to the central and south side, and for lowering water levels immediately south of the
646 islands as winds blow offshore. The spatial differences between 2011 and 2016 led to Horn Island
647 having a subaerial areal change rate of $+0.05 \text{ km}^2/\text{yr}$, a volume change rate of $+4.76 \times 10^5 \text{ m}^3/\text{yr}$,
648 and a shoreline change rate of $-0.8 \text{ m}/\text{yr}$, and Petit Bois Island having a subaerial areal change rate
649 of $-0.002 \text{ km}^2/\text{yr}$, a volume change rate of $+1.25 \times 10^5 \text{ m}^3/\text{yr}$, and a shoreline change rate of -1.5
650 m/yr .

651 *4.3 Morphological Changes Across Entire Study Period: 2004 – 2016*

652 The morphologies and change rates of Horn and Petit Bois islands have only varied
653 moderately during the entire study period, as both were exposed to the same mean wave energies,
654 wind speeds, and sea level rise rate of $+0.004 \text{ mm}/\text{yr}$ between 2004 and 2016 (NOAA Tide Gauge
655 8735180 at Dauphin Island, AL, 2018). Horn Island exhibited net erosional trends to its subaerial
656 area, volume, and shorelines, and to its subaqueous nearshore sediment volume. Net topographic
657 sediment loss on Horn Island, between 2004 and 2016, occurred at an average rate of -4.29×10^5
658 m^3/yr , most of which occurred on the island's interior dunes and tips. Horn Island's average
659 subaerial area and total average shoreline change rates were relatively small for the overall study
660 period, $-0.07 \text{ km}^2/\text{yr}$ and $-2 \text{ m}/\text{yr}$ respectively.

661 Petit Bois Island also exhibited net erosional trends between 2004 and 2016. The average
662 rate of change to Petit Bois' subaerial area was $-0.03 \text{ km}^2/\text{yr}$, while its shoreline change rate was
663 $-3.1 \text{ m}/\text{yr}$, and its subaerial sediment volume change rate was $-1.23 \times 10^4 \text{ m}^3/\text{yr}$. In addition to
664 these trends, Petit Bois Island somewhat reoriented during this period and experienced in-place

665 island narrowing and lengthening. The extent of this in-place narrowing on Petit Bois' south-
666 central and southeastern shorelines are shown in transects PB2 (Fig. 16) and PB3 (Fig. 17). The
667 rates at which the shoreline retreated between 2004 and 2016 on transect PB2 was ~10 m/yr, and
668 on PB3 was ~8 m/yr.

669 Mean wind speeds (P1: 5.29 ± 2.9 m/s; P2: 5.16 ± 2.7 m/s; P3: 5.45 ± 2.5 m/s; P4: $5.16 \pm$
670 2.5 m/s; P5: 5.33 ± 2.6 m/s) of the study periods did not vary significantly, thus they did not appear
671 to have a direct correlation with observed spatial changes on Horn and Petit Bois islands. There
672 also did not appear to be a correlation with respect to mean wind speed and accretion/erosion. It
673 was observed, however, that for periods where the dominant wind direction was out of the SE,
674 erosion occurred, and when the dominant direction was out of the ENE, accretion occurred.

675 Several clear trends were observed with regards to wave energies and their effects on the
676 islands' geomorphologies. First, the highest mean wave energy (0.485 ± 1.44 kJ/m²) for a single
677 period was observed in period 1 (2004-05). During this period, both Horn and Petit Bois islands
678 experienced the largest amounts of erosion and land loss to their areas and volumes. Second, when
679 the islands experienced instances of wave energies >10 kJ/m², accompanying storm surge heights
680 of at least 1 m generated erosion to low-lying areas of Horn and Petit Bois islands.

681 **4.4 Overall Trends**

682 Area and shoreline positions of the MS-AL barrier islands have been surveyed since the
683 1800's. Figure 25 shows the historical subaerial area sizes of Horn and Petit Bois islands since
684 1848/49, indicating negative trends. Horn Island has lost ~3 to 3.5 km² in the past ~170 years,
685 while Petit Bois Island has lost ~4 to 4.5 km² in the same amount of time (Waller and Malbrough,
686 1976; Byrnes et al, 1991; Morton, 2007, 2008; Carter et al., 2018), including data from this study.
687 Short-term areal change rates found during this study were -0.07 km²/yr for Horn Island and -0.03

688 km²/yr for Petit Bois Island. These values were within an order of magnitude of previous results
689 between 1986 and 1998 (Morton, 2007). Short-term changes of shoreline positions of the MS
690 barrier islands were also measured at a mean rate of -2.1 m/yr, between 1986 and 2001 (Morton
691 et al., 2004). In this study, Horn Island's shoreline change rate was -2 m/yr and Petit Bois Island's
692 rate was -3 m/yr. Since Horn and Petit Bois islands have no history of artificial restorations, island
693 growth or stability is limited by the amount of sediment supplied by natural processes. Byrnes et
694 al. (2013) measured the bathymetric sediment flux of the MS-AL barrier islands between 1917/20
695 and 2005/10 and concluded there was a net deficit of $\sim 3.38 \times 10^5 \text{ m}^3$ between the western ends of
696 Dauphin and Horn islands, though a direct comparison is challenging due to limited bathymetric
697 coverage in our study.

698 Lastly, the geomorphic responses of Horn and Petit Bois islands were compared with those
699 of Ship Island, MS (Fig. 26). All three islands experienced severe erosion from the tropical
700 cyclone impacts of the 2004-05 hurricane seasons. In the years following these storms, Ship Island
701 (2007 to 2012) naturally recovered 0.56 km² (14.4%) of its pre-hurricane Ivan subaerial area
702 (Eisemann et al., 2018); and, from 2005 to 2016 Horn Island recovered 0.88 km² (~6.6%) of its pre-
703 Ivan subaerial area, whereas Petit Bois Island recovered 0.16 km² (~4%) of its pre-Ivan subaerial
704 area. Net topographic and bathymetric sediment volume losses on Ship Island, from 2004 to 2012,
705 were $4.1 \times 10^6 \text{ m}^3$ (average loss 500,000 m³/yr) (Eisemann et al., 2018), whereas between 2004
706 and 2016, net topographic sediment loss on Horn Island was $5.36 \times 10^6 \text{ m}^3$ (average loss of 429,000
707 m³/yr) and on Petit Bois Island net topographic sediment loss was $1.54 \times 10^5 \text{ m}^3$ (average loss of
708 12,300 m³/yr). These trends show Horn, Petit Bois, and Ship islands are responding similarly to
709 sea-level rise, storm impacts, and sediment supply variations over short timescales.

710 5. CONCLUSIONS

711 This study quantified the differences in subaerial area, subaerial sediment volume,
712 bathymetric sediment volume, and shoreline change rates of Horn and Petit Bois islands to
713 understand their geomorphic responses and recoveries to tropical cyclone impacts between 2004
714 and 2016. Horn Island lost a minimum of $6.09 \times 10^6 \text{ m}^3$ of subaerial sediment volume during the
715 high energy events of the 2004-05 hurricane seasons, mainly on its interior dunes, and eastern and
716 western tips. Following these tropical cyclone impacts, Horn Island slowly began rebuilding part
717 of its eastern and western tips, and southern foredunes, yet continued to lose sediment in its interior
718 for an additional six years (2005 to 2011), due to aeolian erosion. Since, Horn Island was only
719 able to recover ~4.3% of the lost subaerial sediment volume (relative to 2004) from 2005 to 2016,
720 it is concluded that the island is no longer stable, and that Holocene shoreface ravinement processes
721 are not contributing significant amounts of sand (Gal, 2018) to the island fast enough to keep pace
722 with the current rate of loss. Petit Bois Island, on the other hand, recouped ~22.9% of its 2004
723 (pre-Ivan) subaerial sediment volume between 2005 and 2016. Most of these gains were to the
724 island's low-lying interior, at the expense of its southern foreshore. Furthermore, because Petit
725 Bois Island's narrow center was only ~240 m in 2016 and narrowing at a rate of ~10 m/yr, the
726 island is vulnerable to breaching during the next storm.

727 Also, when considering the responses of the islands' area and shoreline changes to that of
728 volume changes, the relationship was inconsistent. About 60% of the time, when Horn and Petit
729 Bois islands' areas and shorelines increased or decreased, so did the volume. The other ~40% of
730 the time, the volume change trend was opposite to that of the areas and shorelines. These findings
731 indicate the assessment of an island over sub-decadal timescales cannot be based on a singular
732 parameter (such as either area or volume alone), but that their longevity ultimately depends on
733 both the amount of area an island occupies coupled with the quantity of sediment volume it retains.

734 Furthermore, given that barrier islands globally are declining from various processes,
735 understanding the complex responses of regional barrier island chains in high-resolution remains
736 of the utmost importance for generalized numerical modeling, in addition to management and
737 policy decisions (Dolan and Wallace, 2012).

738

739

ACKNOWLEDGMENTS

740 This work was supported by NOAA Award No. NA16OAR4320199 made to
741 the University of Southern Mississippi Hydrographic Science Research Center. Given this work
742 represents Gremillion's MSc thesis, she would like to thank committee member Dr. Stephan D.
743 Howden for his constructive comments. Others who provided guidance and technical support of
744 this project were Eve Eisemann, Josh Bergeron, the late Admiral (ret.) Kenneth Barbor, Michael
745 Hawkins, and Brian Connon.

746

747

748

749

750

751

752

753

REFERENCES

- 754 Anville, J. B. B. D. & Haye, G. D. L. (1752). Carte de la Louisiane par le Sr. d'Anville. [Paris]
755 [Map] Retrieved on 9 Dec 2018. Accessed from the Library of Congress,
756 <https://www.loc.gov/item/75692506/>.
- 757 Avila, L. A. and Brown, D. P. (2005). Tropical Cyclone Report Tropical Storm Arlene 8-13 June
758 2005. *National Hurricane Center*. Retrieved on 1 May 2018. Accessed from
759 https://www.nhc.noaa.gov/data/tcr/AL012005_Arlene.pdf.

760 Avila, L. A., & Cangialosi, J. (2010). Tropical Cyclone Report Hurricane Ida 4-10 November
761 2009. *National Hurricane Center*. Retrieved on 25 Oct 2018. Accessed from
762 https://www.nhc.noaa.gov/data/tcr/AL112009_Ida.pdf.
763 Bagnold, R. A. (1941). *The physics of blown sand and desert dunes*: Chapman & Hall, London.
764 Bender III, L. C., Guinasso Jr, N. L., Walpert, J. N., & Howden, S. D. (2010). A comparison of
765 methods for determining significant wave heights—Applied to a 3-m discus buoy during
766 Hurricane Katrina. *Journal of atmospheric and oceanic technology*, 27(6), 1012-1028.
767 Retrieved on 4 June 2019. Accessed from
768 <https://journals.ametsoc.org/doi/pdf/10.1175/2010JTECHO724.1>.
769 Berg, R. (2013). Tropical Cyclone Report Hurricane Isaac (AL092012) 21 August–1 September
770 2012. *National Hurricane Center*. Retrieved on 30 Oct 2018. Accessed from
771 https://www.nhc.noaa.gov/data/tcr/AL092012_Isaac.pdf.
772 Bregy, J.C., Wallace, D.J., Minzoni, R.T., & Cruz, V.J. (2018). 2500-year paleotempestological
773 record of intense storms for the northern Gulf of Mexico, United States. *Marine Geology*,
774 396, 26-42. Accessed from <https://doi.org/10.1016/j.margeo.2017.09.009>.
775 Beven, J. (2005). Tropical Cyclone Report Hurricane Dennis 4-13 July 2005. *National*
776 *Hurricane Center*. Retrieved on 25 Oct 2018. Accessed from
777 https://www.nhc.noaa.gov/data/tcr/AL042005_Dennis.pdf.
778 Brown, D. P. (2011). Tropical Cyclone Report Tropical Storm Lee (AL132011) 2-5
779 September 2011. *National Hurricane Center*. Retrieved on 29 Oct 2018. Accessed from
780 https://www.nhc.noaa.gov/data/tcr/AL132011_Lee.pdf.
781 Buijsman, M. C., Sherwood, C. R., Gibbs, A. E., Gelfenbaum, G., Kaminsky, G.,
782 Ruggiero, P., & Franklin, J. (2003). Regional sediment budget of the Columbia River
783 littoral cell, USA, Analysis of Bathymetric-and Topographic-Volume Change. *US*
784 *Geological Survey Open-File Report*, 02-281. Retrieved on 29 Oct 2018. Accessed from
785 <https://pubs.usgs.gov/of/2002/of02-281/>.
786 Byrnes, M. R., McBride, R. A., Penland, S., Hiland, M. W., & Westphal, K. A. (1991).
787 Historical changes in shoreline position along the Mississippi Sound barrier islands.
788 In *GCSSEPM Foundation Twelfth Annual Research Conference Program and*
789 *Abstracts* (pp. 43-55).
790 Byrnes, M. R., Rosati, J. D., Griffiee, S. F., & Berlinghoff, J. L. (2013). Historical sediment
791 transport pathways and quantities for determining an operational sediment budget:
792 Mississippi Sound barrier islands. *Journal of Coastal Research*, 63(sp1), 166-183. DOI:
793 10.2112/SI63-014.1.
794 Carter, G. A., Otvos, E. G., Anderson, C. P., Funderburk, W. R., & Lucas, K. L. (2018).
795 Catastrophic storm impact and gradual recovery on the Mississippi-Alabama barrier
796 islands, 2005–2010: Changes in vegetated and total land area, and relationships of post-
797 storm ecological communities with surface elevation. *Geomorphology*, 321, 72-86.
798 Retrieved on 7 Sept 2018. Accessed from
799 <https://www.sciencedirect.com/science/article/pii/S0169555X18303179>.
800 Chaney, P. L. (1999). Extratropical Storms of the Gulf of Mexico and Their Effects Along the
801 Northern Coast of a Barrier Island: West Ship Island, Mississippi.
802 Retrieved on 11 Dec 18. Accessed from
803 http://digitalcommons.lsu.edu/gradschool_disstheses/6884.
804 Cipriani, L. E., & Stone, G. W. (2001). Net longshore sediment transport and textural changes in
805 beach sediments along the southwest Alabama and Mississippi barrier islands,

806 USA. *Journal of Coastal Research*, 17(2), 443-458. West Palm Beach (Florida), ISSN
807 0749-208.

808 Conery, I., Walsh, J. P., & Corbett, D. R. (2018). Hurricane Overwash and Decadal-Scale
809 Evolution of a Narrowing Barrier Island, Ocracoke Island, NC. *Estuaries and*
810 *coasts*, 41(6), 1626-1642. Retrieved on 13 Oct 19. Accessed from
811 <https://link.springer.com/article/10.1007/s12237-018-0374-y>.

812 Dolan, G., & Wallace, D.J. (2012). Policy and management hazards along the Upper Texas
813 coast. *Ocean & Coastal Management*, 59, 77-82. Retrieved on 17 Sept 19. Accessed from
814 <https://doi.org/10.1016/j.ocecoaman.2011.12.021>.

815 Doran, K. S., Stockdon, H. F., Plant, N. G., Sallenger, A. H., Guy, K. K., & Serafin, K. A.
816 (2009). *Hurricane Gustav: observations and analysis of coastal change*. U. S. Geological
817 Survey. Retrieved on 12 March 19. Accessed from
818 [https://www.researchgate.net/profile/Nathaniel_Plant/publication/242252995_Hurricane_](https://www.researchgate.net/profile/Nathaniel_Plant/publication/242252995_Hurricane_Isaac-Observations_and_Analysis_of_Coastal_Change/links/54c257660cf219bbe4e68842.pdf)
819 [Isaac-Observations_and_Analysis_of_Coastal_Change/links/](https://www.researchgate.net/profile/Nathaniel_Plant/publication/242252995_Hurricane_Isaac-Observations_and_Analysis_of_Coastal_Change/links/54c257660cf219bbe4e68842.pdf)
820 [54c257660cf219bbe4e68842.pdf](https://www.researchgate.net/profile/Nathaniel_Plant/publication/242252995_Hurricane_Isaac-Observations_and_Analysis_of_Coastal_Change/links/54c257660cf219bbe4e68842.pdf).

821 Eisemann, E.R., (2016). MODERN FAIR-WEATHER AND STORM SEDIMENT
822 TRANSPORT AROUND SHIP ISLAND, MISSISSIPPI: IMPLICATIONS FOR
823 COASTAL HABITATS AND RESTORATION EFFORTS. *Master's Theses*. 260.
824 Retrieved 1 August 2017. Accessed from http://aquila.usm.edu/masters_theses/260.

825 Eisemann, E. R., Wallace, D. J., Buijsman, M. C., & Pierce, T. (2018). Response of a
826 vulnerable barrier island to multi-year storm impacts: LiDAR-data-inferred
827 morphodynamic changes on Ship Island, Mississippi, USA. *Geomorphology*, 313,
828 58-71. Retrieved on 30 Oct 18. Accessed from
829 <https://doi.org/10.1016/j.geomorph.2018.04.001>.

830 Edwards, B. (2006). Investigation of the effects of detached breakwaters at Holly Beach and
831 Grand Isle, Louisiana. LSU Master's Theses. 3366. Retrieved on 4 Dec 2018. Accessed
832 from https://digitalcommons.lsu.edu/gradschool_theses/3366.

833 Eleuterius, C. K. (1978). Geographical definition of Mississippi Sound. *Gulf and Caribbean*
834 *Research*, 6(2), 179-181. Retrieved on 17 Feb 18. Accessed from
835 <http://aquila.usm.edu/gcr/vol6/iss2/10>.

836 Everitt, B. (2018). West Petit Bois Island Officially Listed. Retrieved 08 Dec 2018.
837 Accessed from <https://www.nps.gov/guis/learn/news/westpetitbois-release.htm>.

838 Fearnley, S. M., Miner, M. D., Kulp, M., Bohling, C., & Penland, S. (2009). Hurricane impact
839 and recovery shoreline change analysis of the Chandeleur Islands, Louisiana, USA: 1855
840 to 2005. *Geo-Marine Letters*, 29(6), 455-466. DOI: 10.1007/s00367-009-0155-5.

841 Foxworth, R. D., Priddy, R. R., Johnson, W. B., & Moore, W. S. (1962). *Heavy Minerals of*
842 *Sand from Recent Beaches of the Gulf Coast of Mississippi and Associated Islands*.
843 Mississippi Geological Survey, Bulletin 93. Retrieved on 14 May 18.
844 Accessed from <https://www.mdeq.ms.gov/wp-content/uploads/2017/06/Bulletin-93.pdf>.

845 Fritz, H. M., Blount, C., Sokoloski, R., Singleton, J., Fuggle, A., McAdoo, B. G., Moore, A.,
846 Grass, C., & Tate, B. (2007). Hurricane Katrina storm surge distribution and field
847 observations on the Mississippi Barrier Islands. *Estuarine, Coastal and Shelf*
848 *Science*, 74(1-2), 12-20. DOI:10.1016/j.ecss.2007.03.015.

849 Froede Jr, C. R. (2006). The impact that Hurricane Ivan (September 16, 2004) made across
850 Dauphin Island, Alabama. *Journal of Coastal Research*, 561-573. DOI:
851 10.2112/05-0438.1.

852 Gabriel, A. O., & Kreutzwiser, R. D. (2000). Conceptualizing environmental stress: A stress-
853 response model of coastal sandy barriers. *Environmental management*, 25(1), 53-69.

854 Gal, N. (2018). Holocene Formation and Evolution of Horn Island, Mississippi, USA.
855 *Master's Theses*, 603. Retrieved on 5 JAN 2019. Accessed from
856 https://aquila.usm.edu/masters_theses/603.

857 Gares, P. A., Wang, Y., & White, S. A. (2006). Using LIDAR to monitor a beach nourishment
858 project at Wrightsville Beach, North Carolina, USA. *Journal of Coastal Research*, 1206-
859 1219. Retrieved on 23 NOV 19. Accessed from
860 <https://www.jcronline.org/doi/full/10.2112/06A-0003.1>.

861 Harter, C., & Figlus, J. (2017). Numerical modeling of the morphodynamic response of a low-
862 lying barrier island beach and foredune system inundated during Hurricane Ike using
863 XBeach and CSHORE. *Coastal Engineering*, 120, 64-74.

864 Hodgson, M. E., & Bresnahan, P. (2004). Accuracy of airborne LiDAR-derived
865 elevation. *Photogrammetric Engineering & Remote Sensing*, 70(3), 331-339.
866 Retrieved on 24 Oct 18. Accessed from <https://doi.org/10.14358/PERS.70.3.331>.

867 Hollis, R. (2018). Late Quaternary Evolution and Stratigraphic Framework Influence on Coastal
868 Systems along the North-Central Gulf of Mexico, USA. *Master's Theses*, 598. Retrieved
869 on 5 January 2019. Accessed from https://aquila.usm.edu/masters_theses/598/.

870 Hollis, R. J., Wallace, D. J., Miner, M. D., Gal, N. S., Dike, C., & Flocks, J. G. (2019). Late
871 Quaternary evolution and stratigraphic framework influence on coastal systems along the
872 north-central Gulf of Mexico, USA. *Quaternary Science Reviews*, 223, 105910.

873 Holthuijsen, L. H. (2007). *Waves in Oceanic and Coastal Waters*. Cambridge university press.
874 Retrieved on 19 Jan 19. Accessed from [http://www.sisal.unam.mx/labeco/
875 LAB_ECOLOGIA/OF_files/82571738-Waves-in-Oceanic-and-Coastal-Waters.pdf](http://www.sisal.unam.mx/labeco/LAB_ECOLOGIA/OF_files/82571738-Waves-in-Oceanic-and-Coastal-Waters.pdf).

876 Howden, S., Gilhousen, D., Guinasso, N., Walpert, J., Sturgeon, M., & Bender, L. (2008).
877 Hurricane Katrina winds measured by a buoy-mounted sonic anemometer. *Journal of*
878 *Atmospheric and Oceanic Technology*, 25(4), 607-616. Retrieved on 4 Jun 19. Accessed
879 from <https://journals.ametsoc.org/doi/full/10.1175/2007JTECHO518.1>

880 Iowa Environmental Mesonet (n.d.) NWS Warning Search by Point or County/Zone.
881 Retrieved on 18 Dec 18. Accessed from
882 <https://mesonet.agron.iastate.edu/vtec/search.php#bypoint/-88.5917/30.2221>.

883 Jevrejeva, S., Moore, J. C., Grinsted, A., Matthews, A. P., & Spada, G. (2014). Trends and
884 acceleration in global and regional sea levels since 1807. *Global and Planetary*
885 *Change*, 113, 11-22. Retrieved on 7 May 18. Accessed from
886 <http://dx.doi.org/10.1016/j.gloplacha.2013.12.004>.

887 Jones, R. (2015). Quantifying extreme weather event impacts on the Northern Gulf Coast using
888 Landsat imagery. *Journal of Coastal Research*, 31(5), 1229-1240.

889 Keen, T. R. (2002). Waves and currents during a winter cold front in the Mississippi bight, Gulf
890 of Mexico: Implications for barrier island erosion. *Journal of Coastal Research*, 622-636.

891 Knabb, R. D., Rhome, J. R., and Brown, D. P. (2005). Tropical Cyclone Report Hurricane
892 Katrina 23—30 August 2005. *National Hurricane Center*. Retrieved on 1 May 2018.
893 Accessed from https://www.nhc.noaa.gov/data/tcr/AL122005_Katrina.pdf.

894 Landsea, C. (2014). Frequently Asked Questions: Why are the strongest winds in a
895 hurricane typically on the right side of the storm? Retrieved on 21 May 2018.
896 Accessed from <http://www.aoml.noaa.gov/hrd/tcfaq/D6.html>.

897 Lentz, E. E., & Hapke, C. J. (2011). Geologic framework influences on the
898 geomorphology of an anthropogenically modified barrier island: assessment of
899 dune/beach changes at Fire Island, New York. *Geomorphology*, 126(1-2), 82-96.
900 doi:10.1016/j.geomorph.2010.10.032.

901 Masetti, R., Fagherazzi, S., & Montanari, A. (2008). Application of a barrier island translation
902 model to the millennial-scale evolution of Sand Key, Florida. *Continental Shelf*
903 *Research*, 28(9), 1116-1126.

904 Masselink, G., & van Heteren, S. (2014). Response of wave-dominated and mixed-
905 energy barriers to storms. *Marine Geology*, 352, 321-347. Retrieved on 21 Jan 19.
906 Accessed from <https://doi.org/10.1016/j.margeo.2013.11.004>.

907 Moore, L. J., List, J. H., Williams, S. J., & Stolper, D. (2007). Modeling barrier island response
908 to sea-level rise in the Outer Banks, North Carolina. In *Coastal sediments' 07* (pp. 1153-
909 1164).

910 Morton, R. A. (2007). Historical changes in the Mississippi-Alabama barrier islands and the
911 roles of extreme storms, sea level, and human activities. USGS Open-File
912 Report 2007-1161. Retrieved on 9 Sept 2017. Accessed from
913 <https://pubs.usgs.gov/of/2007/1161/OFR-2007-1161-print.pdf>.

914 Morton, R. A. (2008). Historical changes in the Mississippi-Alabama barrier-island chain
915 and the roles of extreme storms, sea level, and human activities. *Journal of*
916 *Coastal Research*, 1587-1600.

917 Morton, R. A. (2010). First-order controls of extreme-storm impacts on the Mississippi-
918 Alabama barrier-island chain. *Journal of Coastal Research*, 635-648.

919 Morton, Robert A., Miller, Tara L., and Moore, Laura J., (2004). National assessment of
920 shoreline change: Part 1: Historical shoreline changes and associated coastal land loss
921 along the U.S. Gulf of Mexico: U.S. Geological Survey Open-file Report 2004-1043,
922 45p. Retrieved on 1 January 2016. Accessed from
923 <https://pubs.usgs.gov/of/2004/1043/ofr-2004-1043.pdf>.

924 Morton, R. A., & Sallenger Jr, A. H. (2003). Morphological impacts of extreme storms on sandy
925 beaches and barriers. *Journal of Coastal Research*, 560-573.

926 National Data Buoy Center (NDBC). (2018). Station 42007 (LLNR) – Biloxi, MS. Retrieved on
927 20 Dec 18. Accessed from https://www.ndbc.noaa.gov/station_page.php?station=42007.

928 National Data Buoy Center (NDBC). (2018). Station 42012 – Orange Beach – Mobile, AL.
929 Retrieved on 20 Dec 18. Accessed from
930 https://www.ndbc.noaa.gov/station_history.php?station=42012.

931 National Data Buoy Center (NDBC). (2018). Station PTBM6 – 8741003 – Petit Bois Island, Port
932 of Pascagoula, MS. Retrieved on 20 Dec 18. Accessed from
933 https://www.ndbc.noaa.gov/station_history.php?station=ptbm6.

934 Nienhuis, J. H., & Lorenzo-Trueba, J. (2019). Simulating barrier island response to sea level rise
935 with the barrier island and inlet environment (BRIE) model v1.0. *Geoscientific Model*
936 *Development*, 12(9), 4013-4030. Retrieved on 1 Nov 2019. Accessed from
937 <https://www.geosci-model-dev.net/12/4013/2019/>.

938 NOAA (2012). Minor Modification to the Saffir-Simpson Hurricane Wind Scale for the
939 2012 Hurricane Season. NOAA National Hurricane Center. Retrieved on 21 Jan 19.
940 Accessed from https://www.nhc.noaa.gov/pdf/sshws_2012rev.pdf.

- 941 NOAA Coastal Services Center. (2012). Lidar 101: An Introduction to Lidar Technology, Data,
942 and Applications. Revised. Charleston, SC: NOAA Coastal Services Center. Retrieved on
943 19 Sept 19. Accessed from <https://coast.noaa.gov/data/digitalcoast/pdf/lidar-101.pdf>.
- 944 NOAA Tide Gauge 8735180 Dauphin Island, Alabama (2018). Relative Sea Level Trend.
945 Retrieved on 20 March 2019. Accessed from
946 https://tidesandcurrents.noaa.gov/sltrends/sltrends_station.shtml?id=8735180.
- 947 OCM Partners. (2017). 2004 US Army Corps of Engineers (USACE) Topo/Bathy Lidar:
948 Alabama, Florida, Mississippi and North Carolina from 2004-04-021 to 2004-09-25.
949 NOAA National Centers for Environmental Information. Retrieved on 1 Apr 2017.
950 Accessed from <https://inport.nmfs.noaa.gov/inport/item/50049>.
- 951 OCM Partners. (2017). 2005 US Army Corps of Engineers (USACE) Post-Hurricane Katrina
952 Topo/Bathy Project for the Alabama, Florida, Louisiana and Mississippi Coasts from
953 2005-10-12 to 2005-12-11. NOAA National Centers for Environmental Information.
954 Retrieved on 1 Apr 2017. Accessed from <https://inport.nmfs.noaa.gov/inport/item/50056>.
- 955 OCM Partners. (2017). 2007 USGS/NPS/NASA Experimental Advanced Airborne Research
956 Lidar (EAARL): Northern Gulf of Mexico Barrier Islands from 2007-06-27 to 2007-06-
957 30. NOAA National Centers for Environmental Information. Retrieved on 1 Apr 2017.
958 Accessed from <https://inport.nmfs.noaa.gov/inport/item/50105>.
- 959 OCM Partners. (2017). 2011 U.S. Army Corps of Engineers (USACE) Topographic LiDAR:
960 Alabama, Mississippi and Louisiana from 2011-05-31 to 2011-06-04. NOAA National
961 Centers for Environmental Information. Retrieved on 1 Apr 2017. Accessed from
962 <https://inport.nmfs.noaa.gov/inport/item/50017>.
- 963 OCM Partners. (2017). 2016 USACE NCMP Topobathy Lidar DEM: Gulf Coast (AL, FL, MS,
964 TX) from 2016-07-23 to 2016-10-10. NOAA National Centers for Environmental
965 Information. Retrieved on 1 Apr 2017. Accessed from
966 <https://inport.nmfs.noaa.gov/inport/item/49427>.
- 967 Odezulu, C. I., Lorenzo-Trueba, J., Wallace, D. J., & Anderson, J. B. (2018). Follets
968 Island: a case of unprecedented change and transition from rollover to subaqueous shoals.
969 In *Barrier Dynamics and Response to Changing Climate* (pp. 147-174). Springer, Cham.
- 970 Otvos, E. G. (1979). Barrier island evolution and history of migration, north central Gulf
971 Coast. *Barrier islands from the Gulf of St. Lawrence to the Gulf of Mexico*, 291-319.
- 972 Otvos, E.G. (1981). Barrier island formation through nearshore aggradation-stratigraphic
973 field evidence. *Marine Geology*, 43, 195-243.
- 974 Otvos, E. G. (1985). Barrier platforms: northern Gulf of Mexico. *Marine Geology*, 63(1-4), 285-
975 305.
- 976 Otvos, E. G. (2001). Mississippi coast: stratigraphy and Quaternary evolution in the Northern
977 Gulf Coastal Plain framework. *Stratigraphic and Paleontologic Studies of the Neogene
978 and Quaternary Sediments in Southern Jackson County, Mississippi. US Geological
979 Survey Open File Report*, 01-415. Retrieved on 24 Apr 17. Accessed from
980 <https://pubs.usgs.gov/of/2001/of01-415/chap8txt.pdf>.
- 981 Otvos, E. G. (2005). Coastal barriers, Gulf of Mexico: Holocene evolution and
982 chronology. *Journal of Coastal Research*, 141-163.
- 983 Otvos, E.G. (2018). Coastal barriers, northern Gulf-Last Eustatic Cycle; genetic categories
984 and development contrasts. A review. *Quaternary Science Reviews*, 193, 212-243.

- 985 Otvos, E. G., & Carter, G. A. (2008). Hurricane degradation—barrier development cycles,
986 northeastern Gulf of Mexico: landform evolution and island chain history. *Journal of*
987 *Coastal Research*, 463-478. DOI: 10.2112/06-0820.1.
- 988 Otvos, E. G., & Carter, G. A. (2013). Regressive and transgressive barrier islands on the North-
989 Central Gulf Coast—Contrasts in evolution, sediment delivery, and island
990 vulnerability. *Geomorphology*, 198, 1-19. Retrieved on 10 Dec 2018. Accessed
991 from <http://dx.doi.org/10.1016/j.geomorph.2013.05.015>.
- 992 Pereira-Valadés, D. (2015). WindRose v1.3.1.0. Mathworks. Retrieved on 2 Nov 19. Accessed
993 from [https://www.mathworks.com/matlabcentral/fileexchange/47248-wind-](https://www.mathworks.com/matlabcentral/fileexchange/47248-wind-rose?s_tid=FX_rc1_behav)
994 [rose?s_tid=FX_rc1_behav](https://www.mathworks.com/matlabcentral/fileexchange/47248-wind-rose?s_tid=FX_rc1_behav).
- 995 Priestas, A. M., & Fagherazzi, S. (2010). Morphological barrier island changes and recovery of
996 dunes after Hurricane Dennis, St. George Island, Florida. *Geomorphology*, 114(4), 614-
997 626. Zhang, K., Whitman, D., Leatherman, S., & Robertson, W. (2005). Quantification of
998 beach changes caused by Hurricane Floyd along Florida's Atlantic coast using airborne
999 laser surveys. *Journal of Coastal Research*, 123-134.
- 1000 Rodriguez, A. B., Yu, W., & Theuerkauf, E. J. (2018). Abrupt increase in washover
1001 deposition along a transgressive barrier island during the late nineteenth century
1002 acceleration in sea-level rise. In *Barrier Dynamics and Response to Changing*
1003 *Climate* (pp. 121-145). Springer, Cham.
- 1004 Sallenger Jr, A. H. (2000). Storm impact scale for barrier islands. *Journal of Coastal*
1005 *Research*, 16(3).
- 1006 Salzmann, L., Green, A., & Cooper, J. A. G. (2013). Submerged barrier shoreline
1007 sequences on a high energy, steep and narrow shelf. *Marine Geology*, 346, 366-374.
1008 Retrieved on 4 Dec 18. Accessed from <https://doi.org/10.1016/j.margeo.2013.10.003>.
- 1009 Saye, S. E., Van der Wal, D., Pye, K., & Blott, S. J. (2005). Beach–dune morphological
1010 relationships and erosion/accretion: an investigation at five sites in England and Wales
1011 using LIDAR data. *Geomorphology*, 72(1-4), 128-155. Retrieved on 22 Nov 19.
1012 Accessed from
1013 <https://www.sciencedirect.com/science/article/abs/pii/S0169555X05001698>.
- 1014 Schmid, K. (2003). *East Ship Island Evolution, Morphology, and Hurricane Response—*
1015 *1994 to 2001*. Mississippi Department of Environmental Quality, Office of Geology,
1016 Coastal Section, Energy and Coastal Geology Division. Retrieved on 5 Dec 17. Accessed
1017 from [https://geology.deq.ms.gov/coastal/NOAA_DATA/Publications/Publications/](https://geology.deq.ms.gov/coastal/NOAA_DATA/Publications/Publications/Barrier_Islands/Open%20File%2020134.pdf)
1018 [Barrier_Islands/Open%20File%2020134.pdf](https://geology.deq.ms.gov/coastal/NOAA_DATA/Publications/Publications/Barrier_Islands/Open%20File%2020134.pdf).
- 1019 Sciaudone, E. J., Velasquez-Montoya, L., Smyre, E. A., & Overton, M. F. (2016). Spatial and
1020 temporal variability in dune field: Pea Island, North Carolina. *Shore & Beach*, 84(2), 49-
1021 58.
- 1022 Stewart, S. R. (2004). Tropical Cyclone Report Hurricane Ivan 2-24 September 2004.
1023 *National Hurricane Center*. Retrieved on 1 May 2018. Accessed from
1024 https://www.nhc.noaa.gov/data/tcr/AL092004_Ivan.pdf.
- 1025 Stewart, S. R. (2006). Tropical Cyclone Report Hurricane Cindy 3-7 July 2006. *National*
1026 *Hurricane Center*. Retrieved on 1 May 2018. Accessed from
1027 https://www.nhc.noaa.gov/data/tcr/AL032005_Cindy.pdf.
- 1028 Stone, G. W., Liu, B., Pepper, D. A., & Wang, P. (2004). The importance of extratropical
1029 and tropical cyclones on the short-term evolution of barrier islands along the
1030 northern Gulf of Mexico, USA. *Marine Geology*, 210(1-4), 63-78.

- 1031 doi:10.1016/j.margeo.2004.05.021.
- 1032 Storm Prediction Center (n.d.). Beaufort Wind Scale. Retrieved on 29 Jan 19. Accessed from
1033 <https://www.spc.noaa.gov/faq/tornado/beaufort.html>.
- 1034 Thieler, E. R., Himmelstoss, E. A., Zichichi, J. L., & Ergul, A. (2009). *The Digital Shoreline*
1035 *Analysis System (DSAS) version 4.0-an ArcGIS extension for calculating shoreline*
1036 *change* (No. 2008-1278). US Geological Survey. Retrieved on 18 Jun 17. Accessed from
1037 https://woodshole.er.usgs.gov/project-pages/DSAS/version4/data/DSASv4_3.pdf.
- 1038 Thomason, R. (2016). Biloxi Marsh Platform Response due to Meteorological Forcing.
1039 *University of New Orleans Theses and Dissertations*. 2280. Retrieved on 7 Jun 2017.
1040 Accessed from [https://scholarworks.uno.edu/cgi/viewcontent.cgi?](https://scholarworks.uno.edu/cgi/viewcontent.cgi?referer=https://scholar.google.com/&httpsredir=1&article=3367&context=td)
1041 [https://scholarworks.uno.edu/cgi/viewcontent.cgi?](https://scholarworks.uno.edu/cgi/viewcontent.cgi?referer=https://scholar.google.com/&httpsredir=1&article=3367&context=td)
1042 Twichell, D. C., Flocks, J. G., Pendleton, E. A., & Baldwin, W. E. (2013). Geologic controls on
1043 regional and local erosion rates of three northern Gulf of Mexico barrier-island
1044 systems. *Journal of Coastal Research*, 63(sp1), 32-45. DOI: 10.2112/SI63-004.
- 1045 Walsh, K. J., McBride, J. L., Klotzbach, P. J., Balachandran, S., Camargo, S. J., Holland,
1046 G., Klotzbach, P. J., Knutson, T. R., Kossin, J. P., Lee, T., Sobel, A. & Sugi, M. (2016).
1047 Tropical cyclones and climate change. *Wiley Interdisciplinary Reviews: Climate*
1048 *Change*, 7(1), 65-89. DOI: 10.1002/wcc.371.
- 1049 Waller, T. H., & Malbrough, L. P. (1976). Temporal Changes in the Offshore Islands of
1050 Mississippi. Mississippi State, Mississippi: Mississippi State University. *Water*
1051 *Resources Institute*, 109p.
- 1052 Xhardé, R., Long, B. F., & Forbes, D. L. (2011). Short-term beach and shoreface evolution on a
1053 cusped foreland observed with airborne topographic and bathymetric LIDAR. *Journal of*
1054 *Coastal Research*, 50-61. Retrieved on 25 Nov 2019. Accessed from
1055 https://www.jcronline.org/doi/abs/10.2112/SI_62_6.
- 1056 Zavala-Hidalgo, J., Romero-Centeno, R., Mateos-Jasso, A., Morey, S. L., & Martinez-Lopez, B.
1057 (2014). The response of the Gulf of Mexico to wind and heat flux forcing: What has been
1058 learned in recent years? *Atmósfera*, 27(3), 317-334.
- 1059 Zhang, K., Whitman, D., Leatherman, S., & Robertson, W. (2005). Quantification of beach
1060 changes caused by Hurricane Floyd along Florida's Atlantic coast using airborne laser
1061 surveys. *Journal of Coastal Research*, 123-134. Retrieved on 19 Sept 19. Accessed from
1062 <https://www.jcronline.org/doi/abs/10.2112/02057.1>.
- 1063

1064 **FIGURE CAPTIONS**

1065 **Figure 1.** Map depicting the north-central Gulf of Mexico coast and the MS-AL barrier island
1066 chain. Modified from ESRI ArcMap v10.5.1.

1067
1068 **Figure 2.** Map depicting Horn Island (left), West Petit Bois Island (middle), and Petit Bois
1069 Island (right). West Petit Bois Island was not included in this study as it is a landform generated
1070 from dredge spoil materials of the Pascagoula Shipping Channel. Imagery from Google Earth
1071 Pro. Inset maps modified from ESRI ArcMap v10.5.1.

1072
1073 **Figure 3.** Digital elevation models of Horn and Petit Bois islands representing island elevation
1074 (topographic and bathymetric) relative to the local mean high water (MHW) datum. The 2004

1075 survey of Horn Island (on the left) is missing $\sim 0.95 \text{ km}^2$, the 2004 survey of Petit Bois Island (on
1076 the right) is missing $\sim 0.62 \text{ km}^2$, and the 2005 Petit Bois survey is missing $\sim 0.22 \text{ km}^2$ of topographic
1077 coverage on the islands' northern sides, indicated by the "missing data" and orange shading over
1078 these land surfaces. These missing 2004 and 2005 areas were artificially filled-in with the orange
1079 shading using Google Earth Pro satellite imagery to show the extent of the missing LIDAR data.
1080 The pink dashed perimeters on the 2004 dataset of Horn and Petit Bois islands represent the
1081 greatest common coverage area available for use in subaerial volume calculations across all five
1082 datasets. Bathymetric coverage was only available for the 2007 dataset (limited to the nearshore)
1083 and the 2016 dataset (up to 14 m MHW depth). Bathymetric volume change calculations were
1084 limited to the greatest coverage area of the 2007 dataset. The color bar depicts elevation, in meters
1085 (m), above or below the local mean high water (MHW) reference datum.

1086
1087 **Figure 4.** Hurricane tracks and wave energy. (Map) Plotted here are the six tropical cyclones that
1088 contributed the largest amounts of wave energy between 2004 and 2016. The light gray circle
1089 denotes the boundary of the 200 km radius around Horn and Petit Bois islands. (Graph) Wave
1090 energy data averaged over 24-hours from Jan. 2004 to Dec. 2016. The blue line graphs are from
1091 NDBC Station 42007, the orange line graphs are from NDBC Station 42012, and the dashed green
1092 line is from NDBC Station 42067-USM3M01 (based on data from Bender et al., 2010). Energy
1093 data for station 42012 were scaled by 0.15 to match station 42007 (from Eisemann et al., 2018).
1094 Time gaps on the graph represent periods of unavailable buoy data.

1095
1096 **Figure 5.** (A) Wind climate of the study area depicted for January 2004 to December 2016 (total
1097 study period). The dominant wind direction was from the SE. (B) Wind climate depicted for July
1098 2011 to December 2016 (anomalous period). The dominant wind direction was from the ENE
1099 during these years, showing a deviation from the expected SE direction. Each wind-rose displays
1100 16 cardinal directions (0° and $360^\circ = \text{N}$) from which wind blew, percent frequency of directions
1101 (represented by petal length), and magnitudes of each speed interval (defined in the legend). Wind
1102 data from January 1, 2004 to December 31, 2008 was obtained from NDBC Station 42007, and
1103 wind data from January 1, 2009 to December 31, 2016 was obtained from NDBC Station PTBM6.

1104
1105 **Figure 6.** Map of transects through Horn Island. H1, H2, and H3 are south trending, cross-shore
1106 transects, and H4 is an east trending, along-shore transect.

1107
1108 **Figure 7.** Elevation profiles for transect H1. The 2004 (blue), 2005 (red), and 2011 (purple)
1109 profiles only contain topographic elevation points. The 2007 (yellow) and 2016 (green) profiles
1110 contain both topographic and bathymetric data points. The cross-shore transect distance originates
1111 in the north (H1) and terminates in the south (H1'). The mean high water (MHW) line is
1112 represented with the dashed blue line at 0 m elevation. The vertical error bar represents $\pm 0.09 \text{ m}$
1113 error.

1114
1115 **Figure 8.** Elevation profiles for transect H2. The 2004 (blue), 2005 (red), and 2011 (purple)
1116 profiles only contain topographic elevation points. The 2007 (yellow) and 2016 (green) profiles
1117 contain both topographic and bathymetric data points. The cross-shore transect distance originates
1118 in the north (H2) and terminates in the south (H2'). The mean high water (MHW) line is
1119 represented with the dashed blue line at 0 m elevation. The vertical error bar represents $\pm 0.09 \text{ m}$
1120 error.

1121
1122
1123
1124
1125
1126
1127
1128
1129
1130
1131
1132
1133
1134
1135
1136
1137
1138
1139
1140
1141
1142
1143
1144
1145
1146
1147
1148
1149
1150
1151
1152
1153
1154
1155
1156
1157
1158
1159
1160
1161
1162
1163
1164

Figure 9. Elevation profiles for transect H3. The 2004 (blue), 2005 (red), and 2011 (purple) profiles only contain topographic elevation points. The 2007 (yellow) and 2016 (green) profiles contain both topographic and bathymetric data points. For the interior lagoon, at 0.2 km in the cross-shore distance, all five datasets contained shallow bathymetry. The cross-shore transect distance originates in the north (H3) and terminates in the south (H3'). The mean high water (MHW) line is represented with the dashed blue line at 0 m elevation. The vertical error bar represents ± 0.09 m error.

Figure 10. Topographic elevation profiles for transect H4. The 2004 (blue), 2005 (red), 2007 (yellow), 2011 (purple), and 2016 (green) profiles contain topographic elevation points. The along-shore transect distance originates in the west (H4) and terminates in the east (H4'). The smoothed black line represents the 500 m running mean across all datasets. The dashed blue line at 0 m elevation represents the mean high water (MHW) line. The vertical error bar represents ± 0.09 m error. Bathymetry is not captured in this set of profiles.

Figure 11. Subaerial elevation differences on Horn Island from 2004 – 2016. This set of images represents differences in elevations (above MHW) at each XYZ point between two corresponding datasets. Differences in elevations were obtained by subtracting the younger year from the older year (ex: 2005 – 2004) and are reported in meters. Positive elevation change (cool colors) represents sediment gain, negative elevation change (warm colors) represents sediment loss. The black color box corresponds to values between -0.5 and 0.5 m elevation change. Elevation gains or losses were then calculated across the total area to yield volumetric change totals in m^3 (Table 5). The white shoreline perimeter in each map represents the most recent shoreline in the set. The 2004 dataset did not have full coverage, thus figures A and E have gray “missing survey coverage” annotations.

Figure 12. Graphs depicting Horn Island's subaerial area (km^2) and subaerial volume (m^3) calculated for each of the five LIDAR datasets: 2004, 2005, 2007, 2011, and 2016. LIDAR-derived subaerial area values, represented by the gray boxes and gray line graph (left y-axis), reflect areal changes for their respective years, minus the $\sim 0.95 km^2$ missing section from the 2004 dataset. LIDAR-derived subaerial volume, represented by the black boxes and black line graph (right y-axis), reflect the areal footprint of the 2004 dataset (pink-dashed perimeter in Fig. 3). The error bars on the subaerial volume data points represent ± 0.09 m error, whereas the error bars on the subaerial area data points represent what the area would be given a ± 0.09 m vertical displacement.

Figure 13. Differences in elevations (below MHW) at each XYZ point between the 2007 and 2016 datasets. Differences in elevations were calculated by subtracting the 2007 values from the 2016 values. Units of change are in meters. Positive change (cool colors) represents sediment gain on the nearshore seafloor, negative change (warm colors) represents sediment loss from the nearshore seafloor, and the black color box corresponds to minimal or no changes. The white shoreline perimeter represents the 2016 shoreline.

1165 **Figure 14.** Map of transects through Petit Bois Island. PB1, PB2, and PB3 are south trending,
1166 cross-shore transects, and PB4 is an east trending, along-shore transect.

1167
1168 **Figure 15.** Elevation profiles for transect PB1. The 2004 (blue), 2005 (red), and 2011 (purple)
1169 profiles only contain topographic elevation points. The 2007 (yellow) and 2016 (green) profiles
1170 contain both topographic and bathymetric data points. The cross-shore transect distance
1171 originates in the north (PB1) and terminates in the south (PB1'). The mean high water (MWH)
1172 line is represented with the dashed blue line at 0 m elevation. The vertical error bar represents
1173 ± 0.09 m error.

1174
1175 **Figure 16.** Elevation profiles for transect PB2. The 2004 (blue), 2005 (red), and 2011 (purple)
1176 profiles only contain topographic elevation points. The 2007 (yellow) and 2016 (green) profiles
1177 contain both topographic and bathymetric data points. The 2005 and 2011 profiles on the south
1178 side of the island do not extend to the MHW line in this transect due to LIDAR survey gaps. The
1179 cross-shore transect distance originates in the north (PB2) and terminates in the south (PB2').
1180 The mean high water (MWH) line is represented with the dashed blue line at 0 m elevation. The
1181 vertical error bar represents ± 0.09 m error.

1182
1183 **Figure 17.** Elevation profiles for transect PB3. The 2004 (blue), 2005 (red), and 2011 (purple)
1184 profiles only contain topographic elevation points. The 2007 (yellow) and 2016 (green) profiles
1185 contain both topographic and bathymetric data points. The 2004 and 2005 datasets have
1186 incomplete survey coverage in the north, and the 2004 and 2011 profiles do not extend to the
1187 MHW line on the south of this transect due to LIDAR survey gaps; the maximum extents
1188 available are plotted above. The cross-shore transect distance originates in the north (PB3) and
1189 terminates in the south (PB3'). The mean high water (MWH) line is represented with the dashed
1190 blue line at 0 m elevation. The vertical error bar represents ± 0.09 m error.

1191
1192 **Figure 18.** Topographic elevation profiles for transect PB4. The 2004 (blue), 2005 (red), 2007
1193 (yellow), 2011 (purple), and 2016 (green) profiles contain topographic elevation points. The along-
1194 shore transect distance originates in the west (PB4) and terminates in the east (PB4'). The
1195 smoothed black line represents the 500 m running mean across all datasets. The dashed blue line
1196 at 0 m elevation represents the mean high water (MWH) line. The vertical error bar represents
1197 ± 0.09 m error. Bathymetry is not captured in this set of profiles.

1198
1199 **Figure 19.** Subaerial elevation differences on Petit Bois Island from 2004 – 2016. This set of
1200 images represents differences in elevations (above MHW) at each XYZ point between two
1201 corresponding datasets. Differences in elevations were obtained by subtracting the younger year
1202 from the older year (ex: 2005 – 2004) and are reported in meters. Positive change (cool colors)
1203 represents sediment gain, negative change (warm colors) represents sediment loss. The black color
1204 box corresponds to values between -0.5 and 0.5 m elevation change. Elevations gains or losses
1205 were then calculated across the total area to yield volumetric totals in m^3 (Table 6). The white
1206 shoreline perimeter in each map represents the most recent shoreline in the set. The 2004 and 2005
1207 datasets did not have full coverage, thus figures A, B, and E have gray “missing survey coverage”
1208 annotations.

1209

1210 **Figure 20.** Petit Bois Island's subaerial area (km²) and subaerial volume (m³) calculated for each
1211 of the five LIDAR datasets: 2004, 2005, 2007, 2011, and 2016. LIDAR-derived subaerial area
1212 values, represented by the gray boxes and gray line graph (left y-axis), reflect areal changes for
1213 their respective years, minus the ~0.62 km² missing section from the 2004 dataset. LIDAR-derived
1214 subaerial volume, represented by the black boxes and black line graph (right y-axis), reflect the
1215 areal footprint of the 2004 dataset (pink-dashed perimeter in Fig. 3). The error bars on the subaerial
1216 volume data points represent ± 0.09 m error, whereas the error bars on the subaerial area data points
1217 represent what the area would be given a ± 0.09 m vertical displacement.

1218
1219 **Figure 21.** Differences in elevations (below MHW) at each XYZ point between the 2007 and 2016
1220 datasets. Differences in elevations were calculated by subtracting the 2007 values from the 2016
1221 values. Units of change are in meters. Positive change (cool colors) represents sediment gain on
1222 the nearshore seafloor, negative change (warm colors) represents sediment loss from the nearshore
1223 seafloor, and the black color box corresponds to minimal or no changes. The white shoreline
1224 perimeter represents the 2016 shoreline.

1225
1226 **Figure 22.** Geomorphic changes on Horn Island's eastern tip between April 2004 and September
1227 2005. Satellite imagery provides a record of geomorphic change between LIDAR surveys, and in
1228 this case shows destabilization of the tip as early as April 2004 and not from a single event.
1229 Imagery from USGS LANDSAT 5 & 7.

1230
1231 **Figure 23.** Washover deposits on Petit Bois Island following Hurricane Katrina. (Top) LIDAR
1232 difference plot between April 2004 and December 2005, with island location inset map and
1233 zoomed-in view. The red and yellow indicates erosion, the green indicates accretion, and the black
1234 indicates 0 to ± 0.5 m change. (Bottom-left) A September 2003 snapshot of Petit Bois Island;
1235 earliest pre-Katrina imagery. (Bottom-right) A snapshot taken 2 days after Hurricane Katrina's
1236 impact in August 2005, showing washover deposits to the interior of the island (scale is same as
1237 2003 image). The red outlines illustrate the location of the foredune which provided ~4,600 m³
1238 source sediment that was overwashed during Hurricane Katrina's storm surge. The green outlines
1239 illustrate where ~2,650 m³ of that sediment was deposited. Imagery from Google Earth Pro.

1240
1241 **Figure 24.** Dune building and lagoon in-filling on Horn Island: 2011 – 2016. (Top) LIDAR
1242 difference plot between June 2011 and October 2016, with island inset map and red box around
1243 the zoomed-in imagery location. The green indicates accretion, the red indicates erosion, and the
1244 black indicates 0 to ± 0.5 m change. On the south-western foredune (in the upper left corner) is an
1245 example of the process of dune building. (Bottom-left) A snapshot of Horn Island taken in
1246 September 2010; closest available to 2011 imagery. The green, transparent shading over the lagoon
1247 is where the sediment will be filled in between 2011 and 2016. (Bottom-right) A snapshot taken
1248 in February 2017, showing evidence, in green shading, where sediment filled-in this part of the
1249 lagoon (scale is same as 2010 image). Imagery from Google Earth Pro.

1250
1251 **Figure 25.** Historical areas of Horn and Petit Bois islands. (Top) Area values of Horn Island from
1252 previously published literature with those of this study. (Bottom) Area values of Petit Bois Island
1253 from previously published literature with those of this study. The 2011 and 2016 (upright triangles)
1254 values represent the total (unclipped) LIDAR-derived area values of Horn and Petit Bois islands

1255 for comparison with other studies. Black squares: Waller and Malbrough, 1976; Gray diamonds:
1256 Byrnes et al., 1991; Gray dots: Morton, 2007 & 2008; Gray inverted triangles: Carter et al., 2018;
1257 Gray upright triangles: Gremillion et al., present study.

1258
1259 **Figure 26.** Comparisons of Horn, Petit Bois, & Ship islands to tropical cyclone impacts. (Top)
1260 LIDAR-derived subaerial area sizes of Horn Island (blue line and left y-axis) with missing ~ 0.95
1261 km^2 , Petit Bois Island (orange line and right y-axis) with missing $\sim 0.62 \text{ km}^2$, and Ship Island (black
1262 line and right y-axis) (Eisemann et al., 2018). (Middle) LIDAR-derived subaerial volumes of Horn
1263 Island (blue line and left y-axis), Petit Bois Island (orange line and right y-axis), and Ship Island
1264 (black line and right y-axis) (Eisemann et al., 2018) all clipped to the greatest geographical
1265 common areas of their respective 2004 datasets. (Bottom) Combined 2004-2016 wave energy
1266 graph and wind-rose diagrams for the 4 periods (gray shading) constraining the LIDAR dataset in
1267 this study.

1268

1269

1270 TABLE CAPTIONS

1271 **Table 1.** Tropical cyclones: 2004 – 2016. Listing and descriptions of tropical cyclones passing
1272 within a 200 km radius of Horn and Petit Bois islands, and the dates of pre- and post-storm LIDAR
1273 datasets used for analyses.

1274

1275 **Table 2.** LIDAR datasets with coverage for both Horn and Petit Bois islands. Uncertainty values
1276 reported by respective agencies are in root mean square error (RMSE). Dataset credit is attributed
1277 to the Joint Airborne Lidar Bathymetry Center of Expertise for 2004, 2005, 2011, and 2016, and
1278 to the U.S. Geological Survey, Florida Integrated Science Center for 2007. *Data sources: OCM
1279 Partners, 2017.

1280

1281 **Table 3.** Wave energy statistics table for each of the five sub-periods, selected to constrain the five
1282 LIDAR datasets. Mean wave energies are averaged over 24-hours (with standard deviation values
1283 to the right of the \pm symbols). Maximum wave energies are based on 24-hour averages. ^A Because
1284 NDBC station 42007 failed six hours prior to Hurricane Katrina's landfall, the maximum wave
1285 energy for P1 was calculated using the maximum significant wave height value of NDBC Station
1286 42067-USM3M01 (from Bender et al., 2010), and the 24-hr average value from Bender et al.
1287 (2010) was calculated into the mean wave energy for P1 and P5.

1288

1289 **Table 4.** Horn Island's Subaerial Area and Shoreline Changes: 2004 – 2016. Values adjusted to
1290 the area of greatest data availability of the 2004 dataset.

1291

1292 **Table 5.** Horn Island's Subaerial Volume Changes: 2004 – 2016. Values adjusted to the greatest
1293 common area defined by shoreline overlap of the 2004 dataset.

1294

1295 **Table 6.** Horn Island's Bathymetric Changes: 2007 – 2016. Values adjusted to the greatest
1296 common bathymetric area of the 2007 dataset.

1297

1298 **Table 7.** Petit Bois Island's Subaerial Area and Shoreline Changes: 2004 – 2016. Values adjusted
1299 to the area of greatest data availability of the 2004 dataset.

1300

1301 **Table 8.** Petit Bois Island's Subaerial Volume Changes: 2004 – 2016. Values adjusted to the
1302 greatest common area defined by shoreline overlap of the 2004 dataset.

1303

1304 **Table 9.** Petit Bois Island's Bathymetric Changes: 2007 – 2016. Values adjusted to the greatest
1305 common bathymetric area of the 2007 dataset.



Mississippi Sound

Horn Island

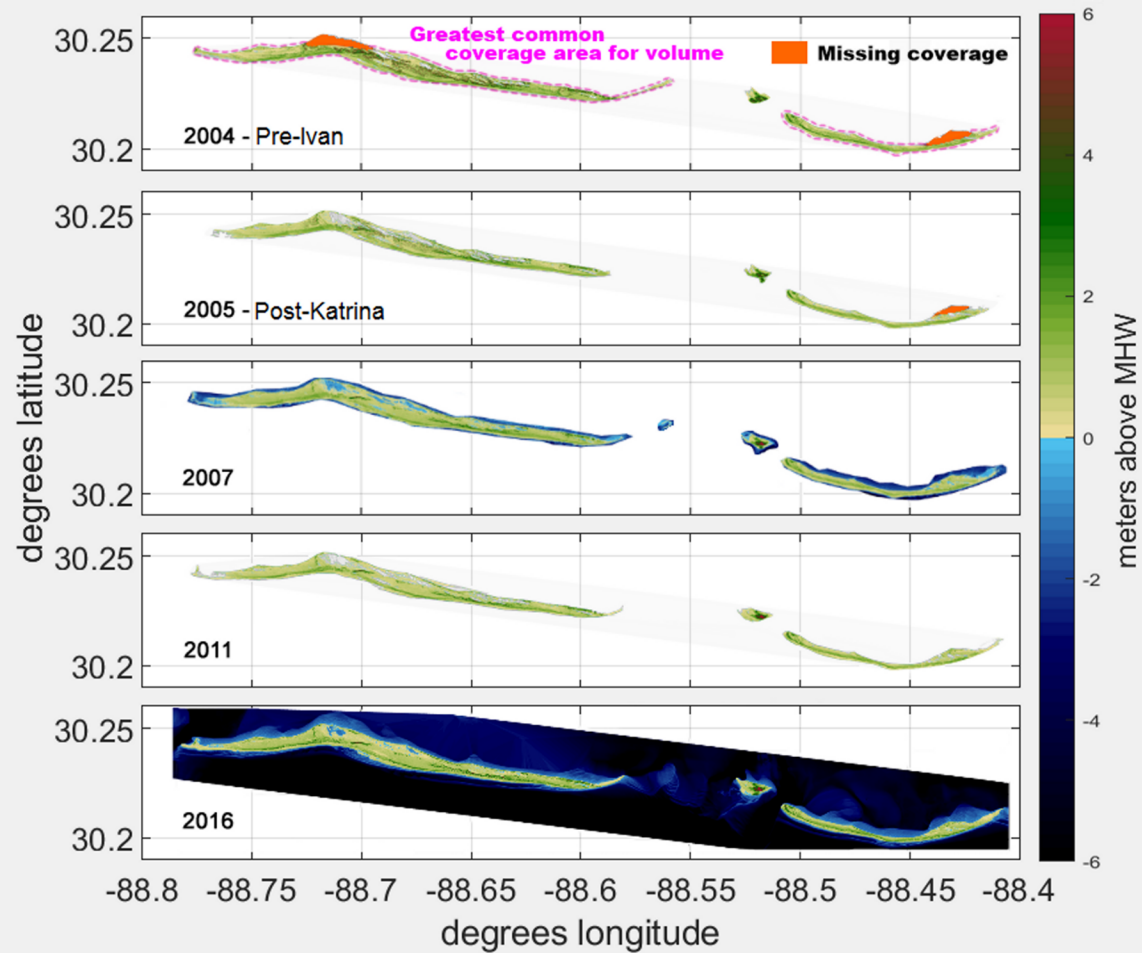
Gulf of Mexico

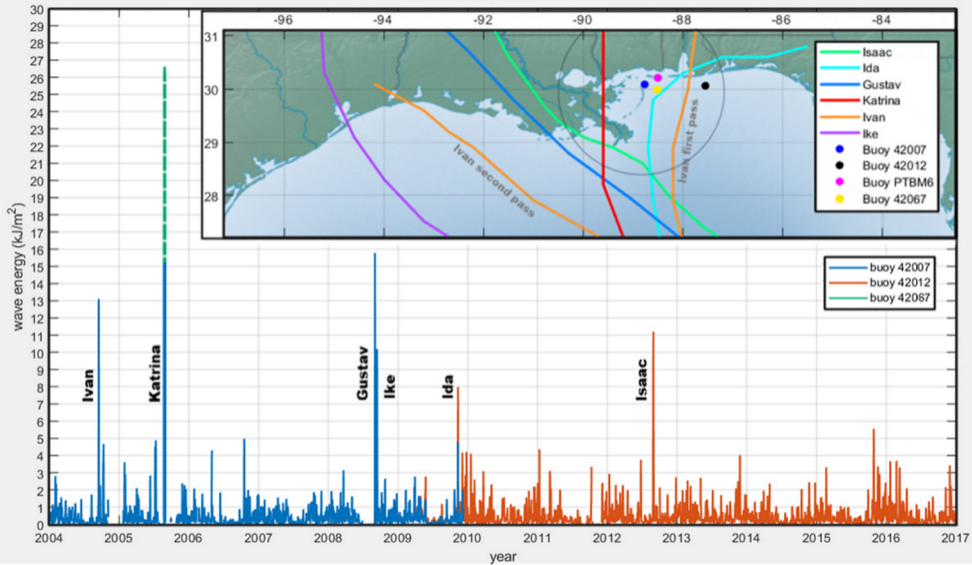


West PBI

Pascagoula Channel

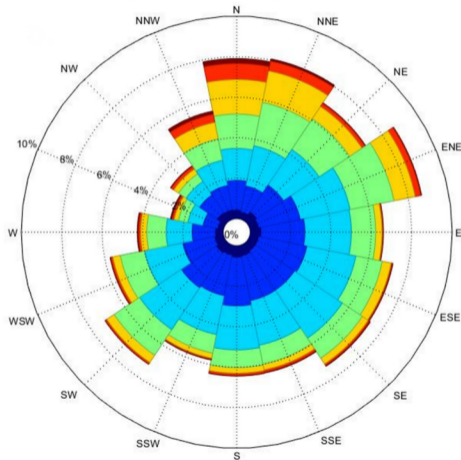
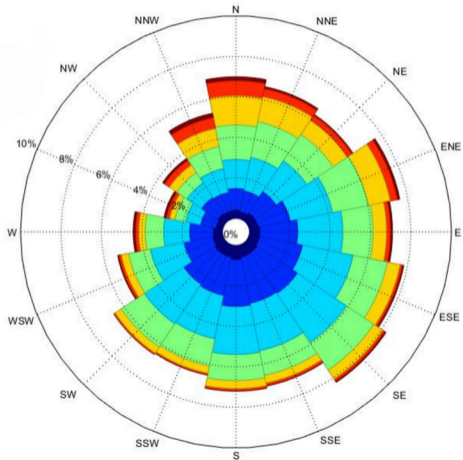
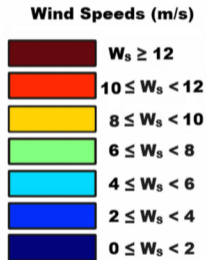
*Petit Bois Island
(PBI)*

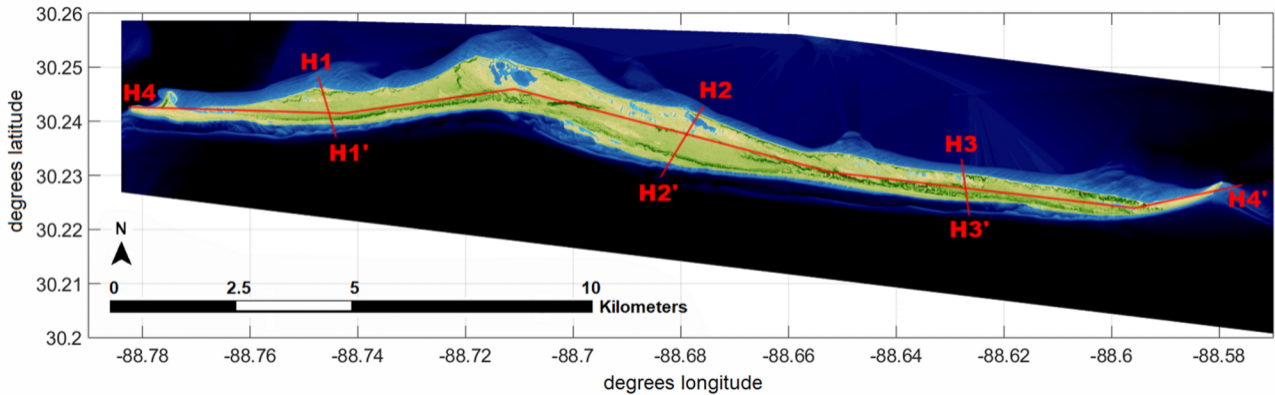


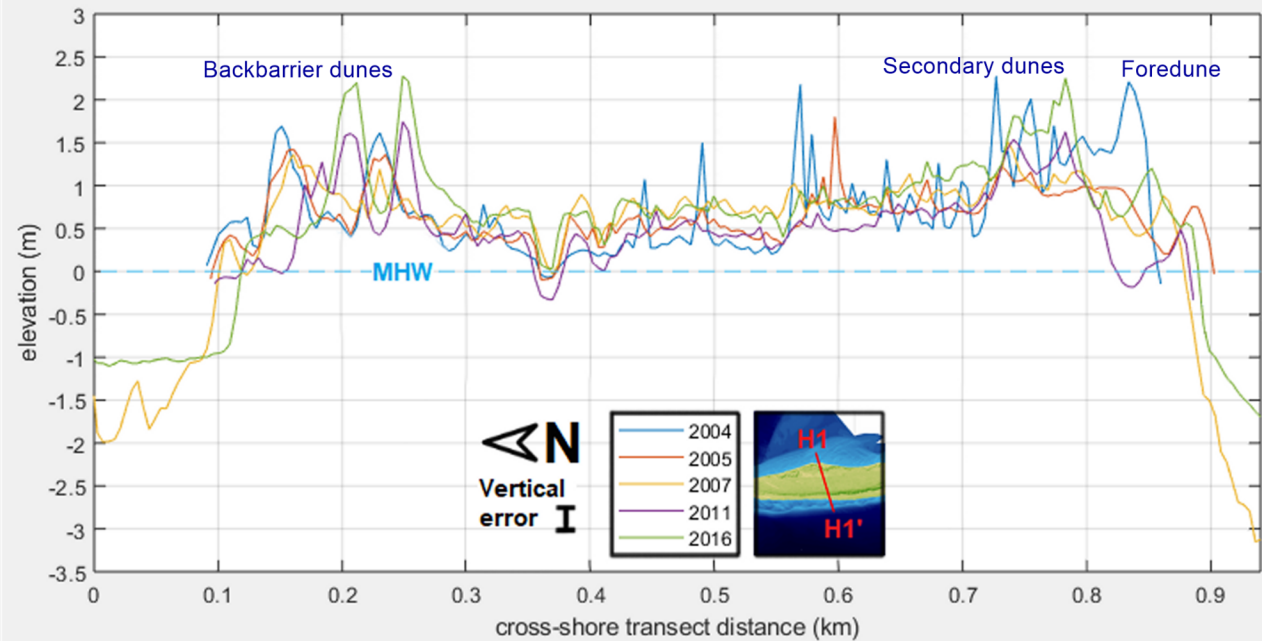


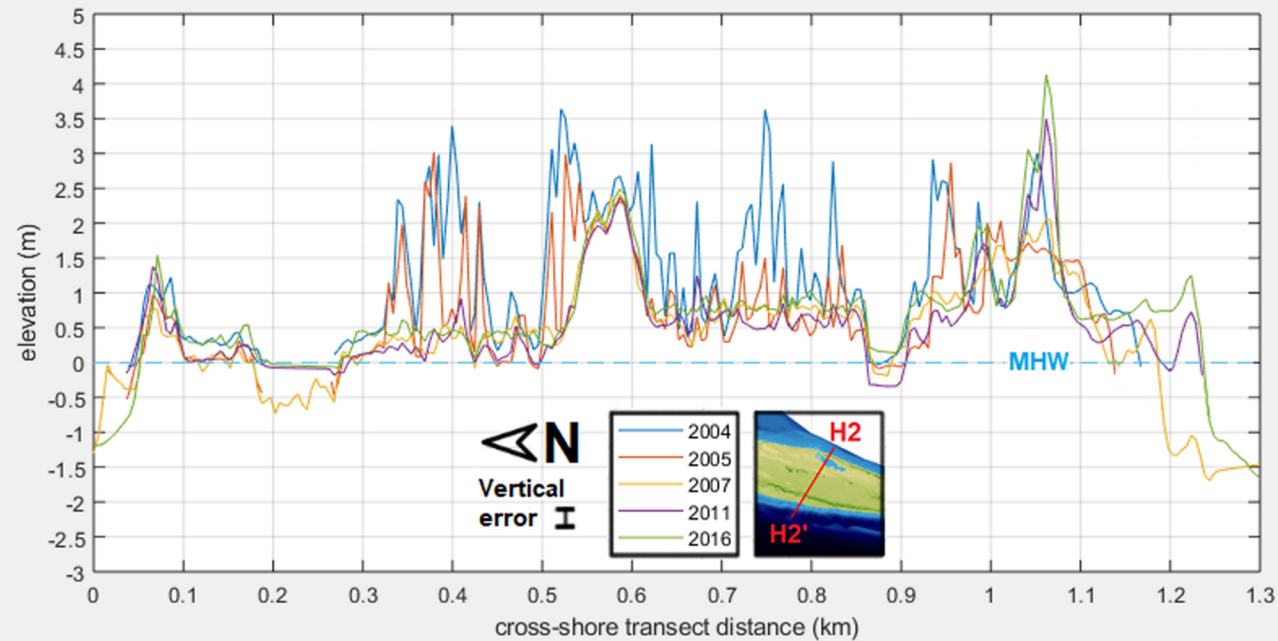
**A. January 1, 2004 - December 31, 2016
(total study period)**

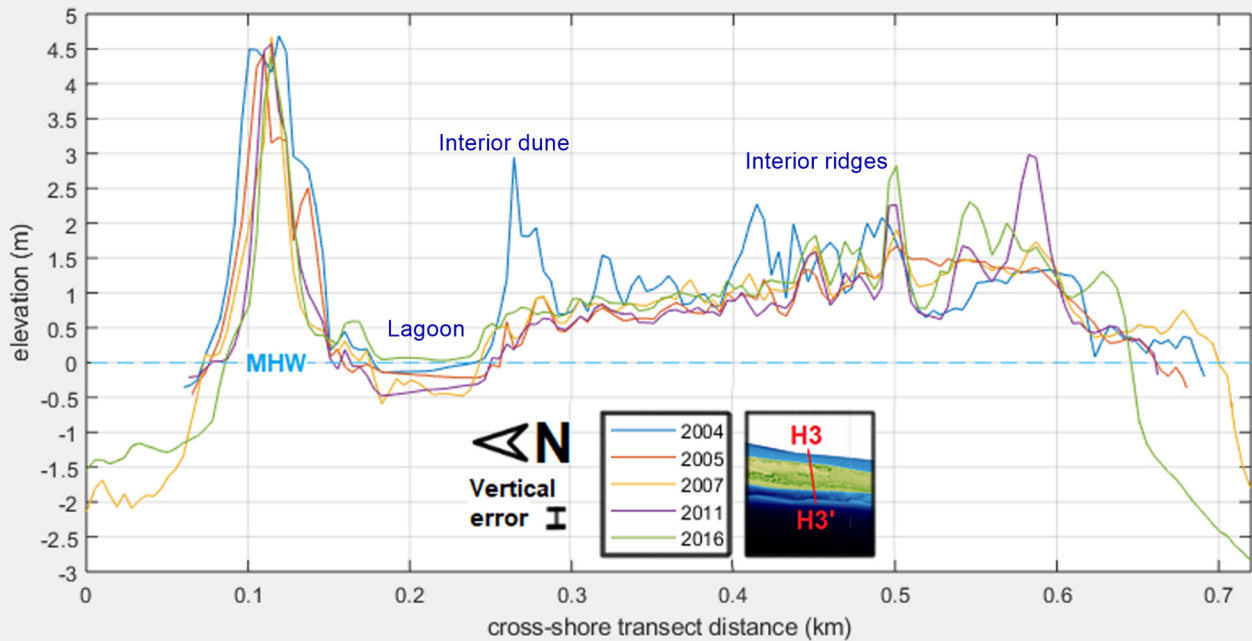
**B. July 1, 2011 - December 31, 2016
(anomalous period)**

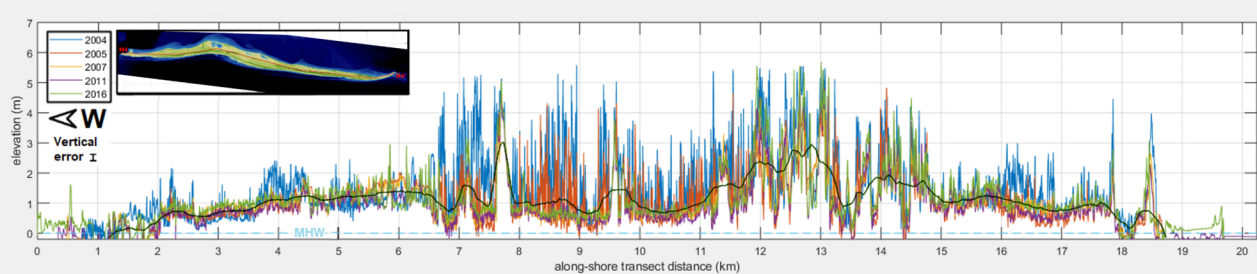


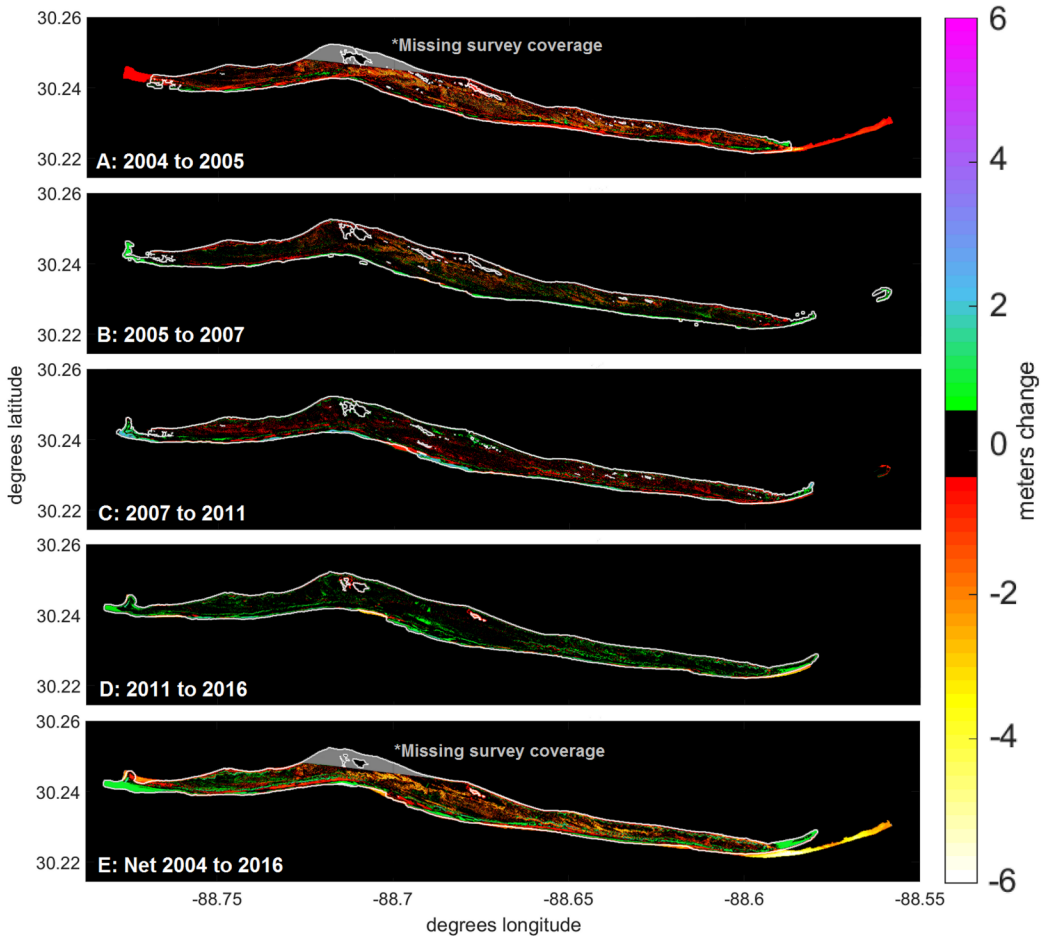


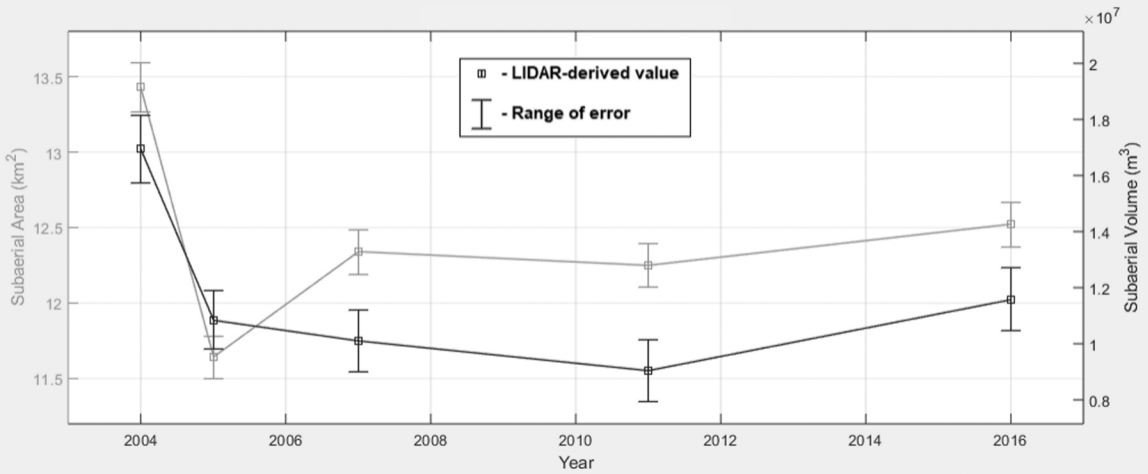


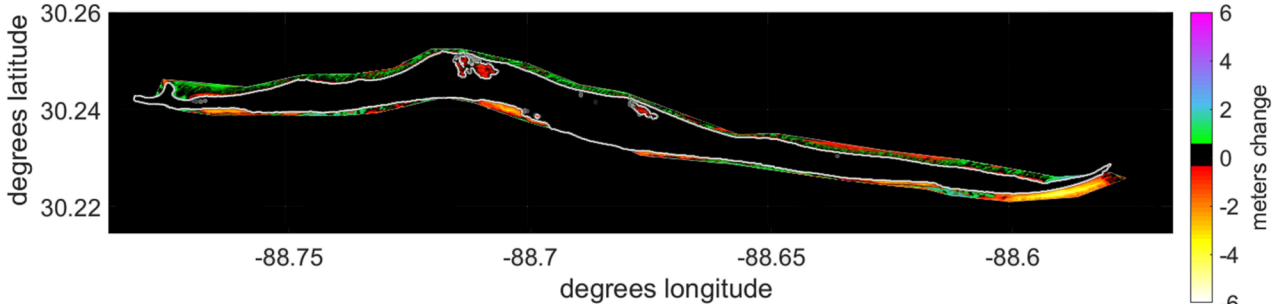


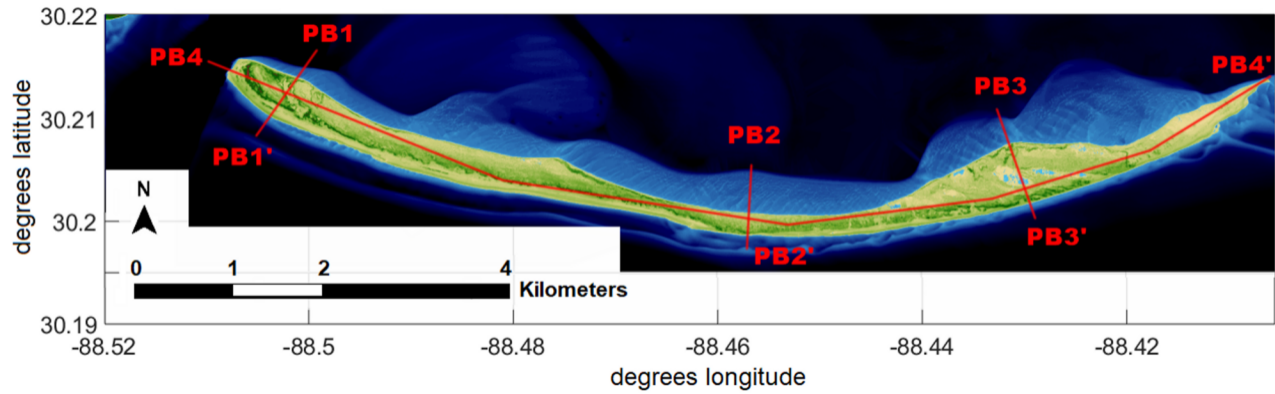


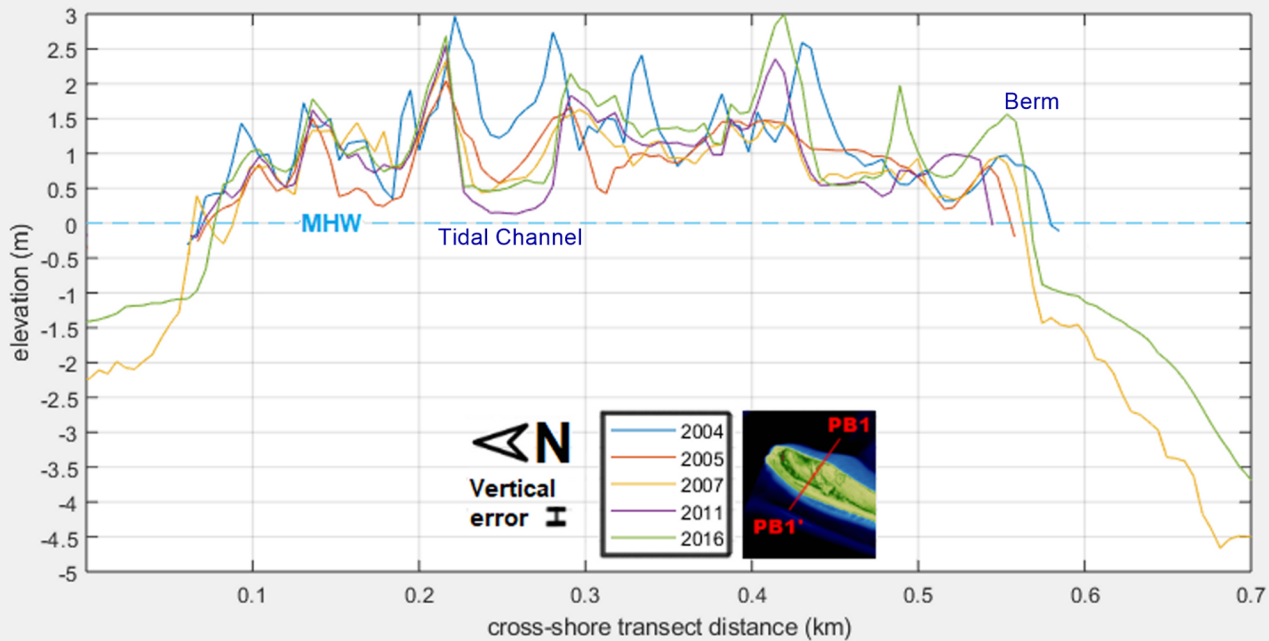


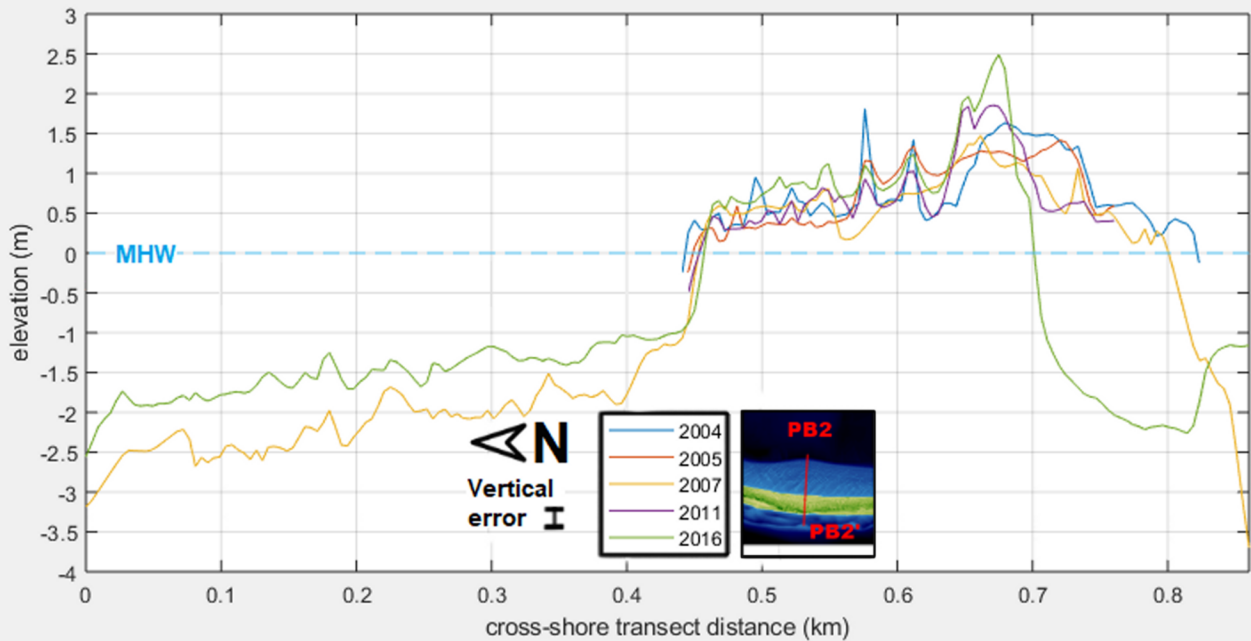


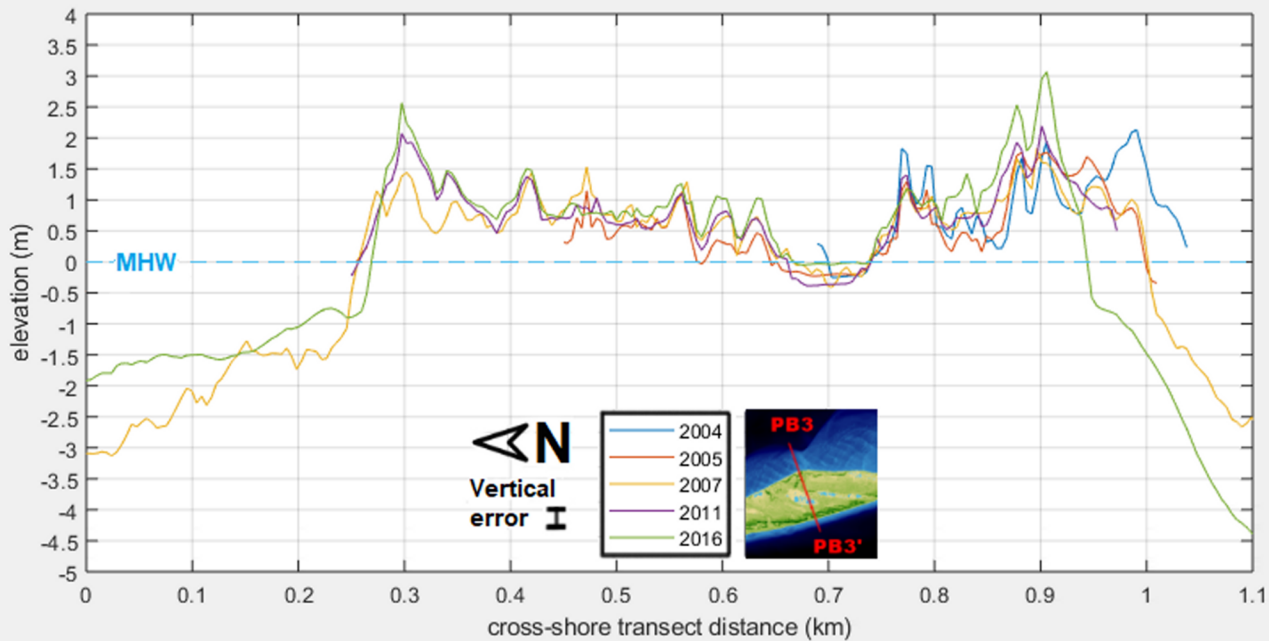


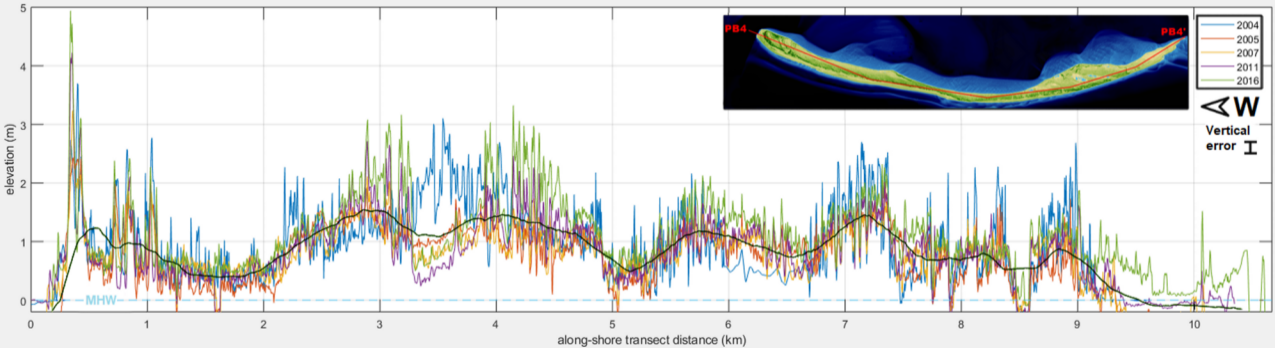


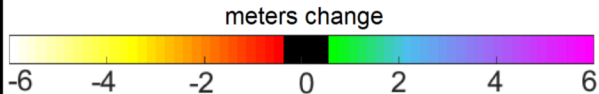
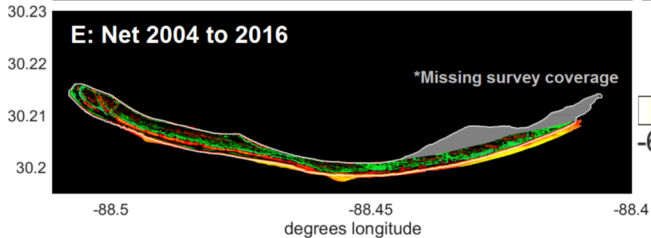
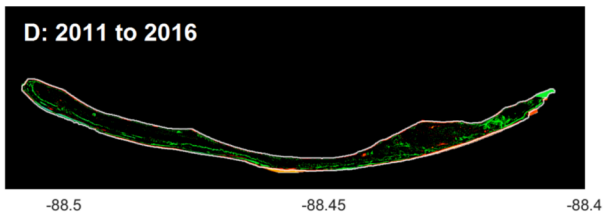
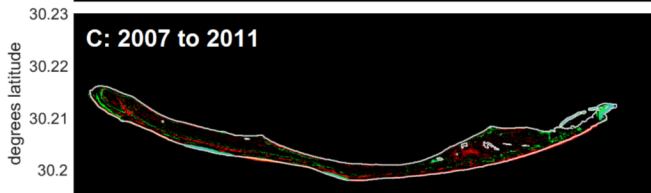
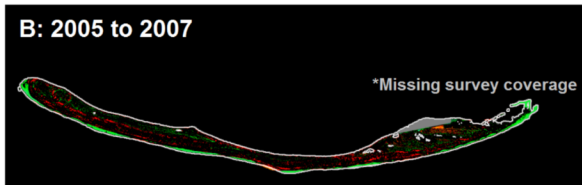
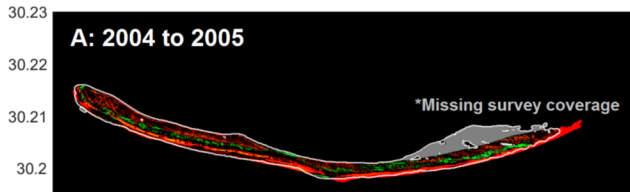


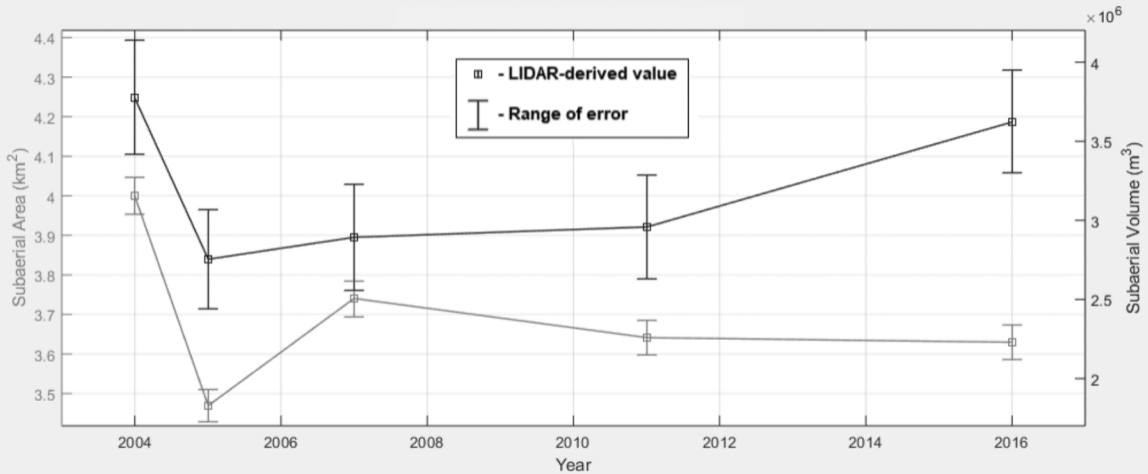


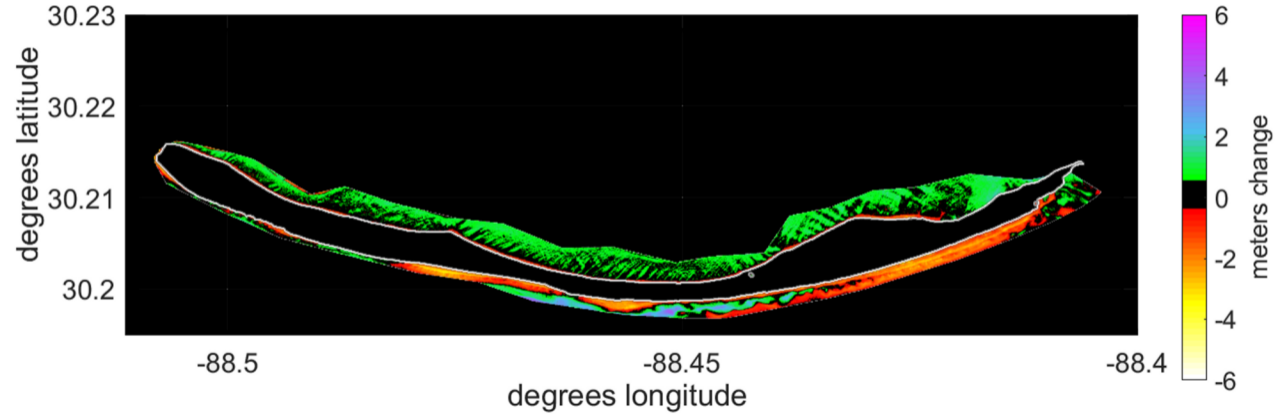


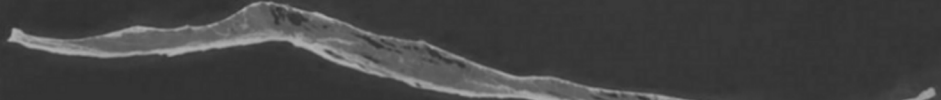




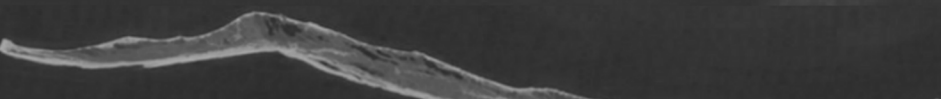








April 2004: Pre-Ivan



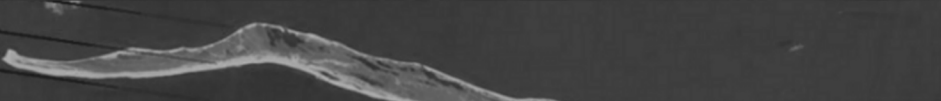
October 2004: Post-Ivan



June 2005: Pre-Dennis



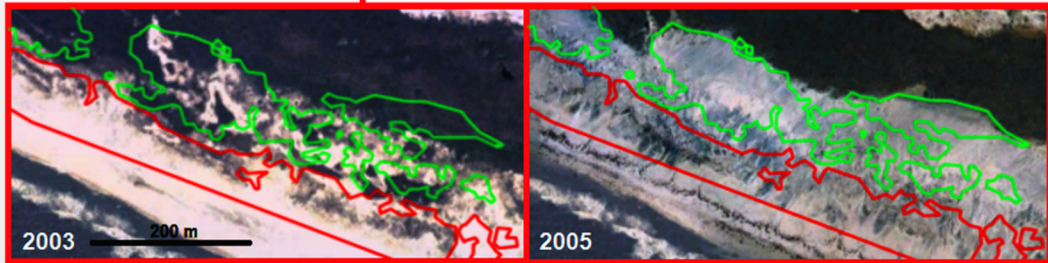
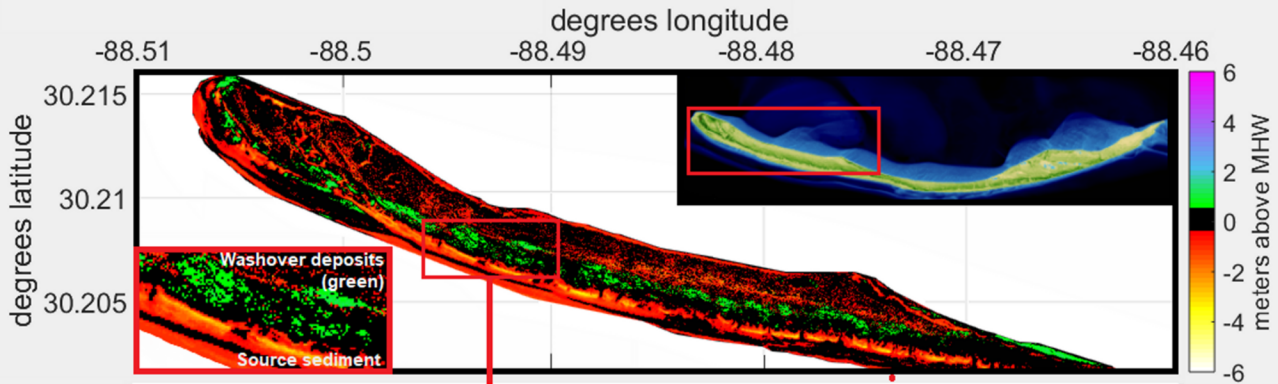
July 2005: Post-Dennis



August 2005: Pre-Katrina



September 2005: Post-Katrina



degrees longitude

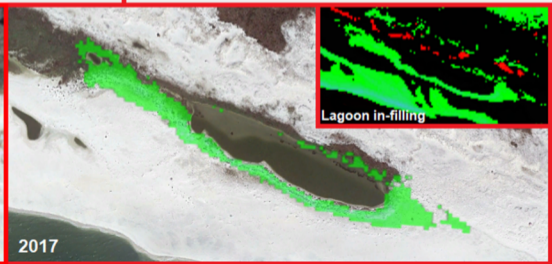
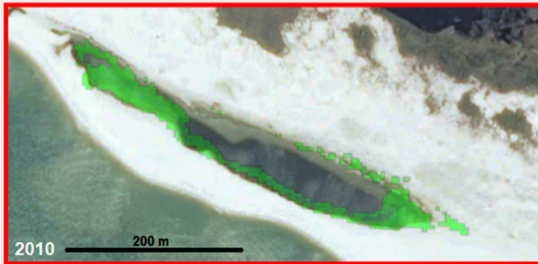
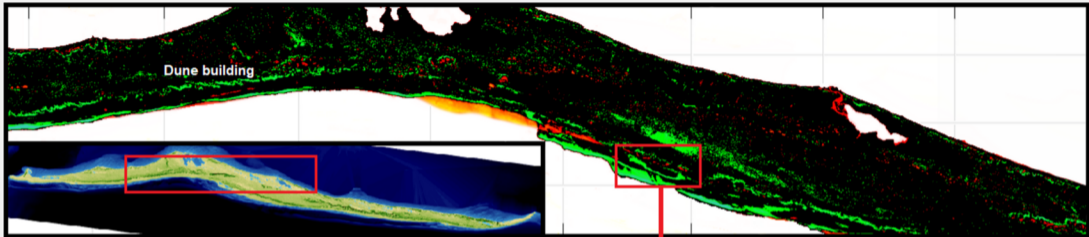
-88.74 -88.73 -88.72 -88.71 -88.7 -88.69 -88.68 -88.67 -88.66

6
4
2
0
-2
-4
-6
meters change

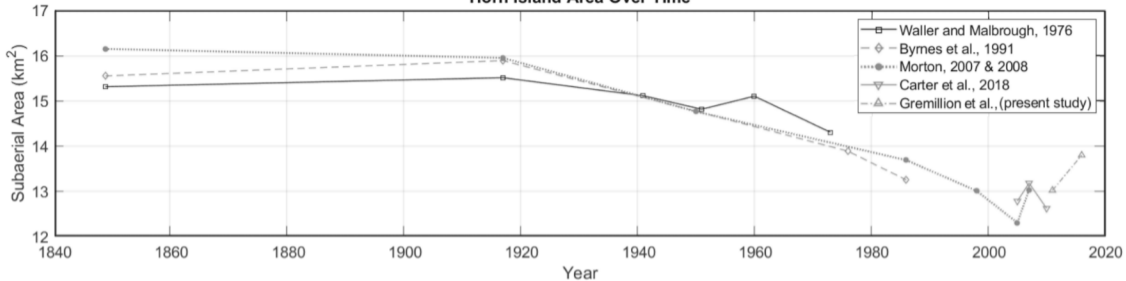
degrees latitude

30.245
30.24
30.235

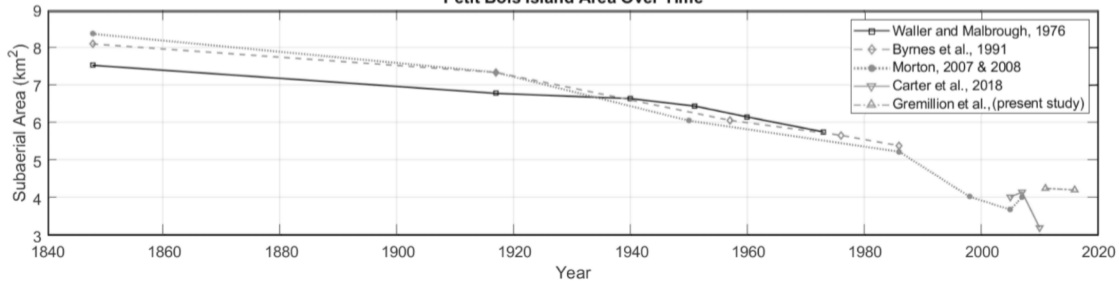
Dune building



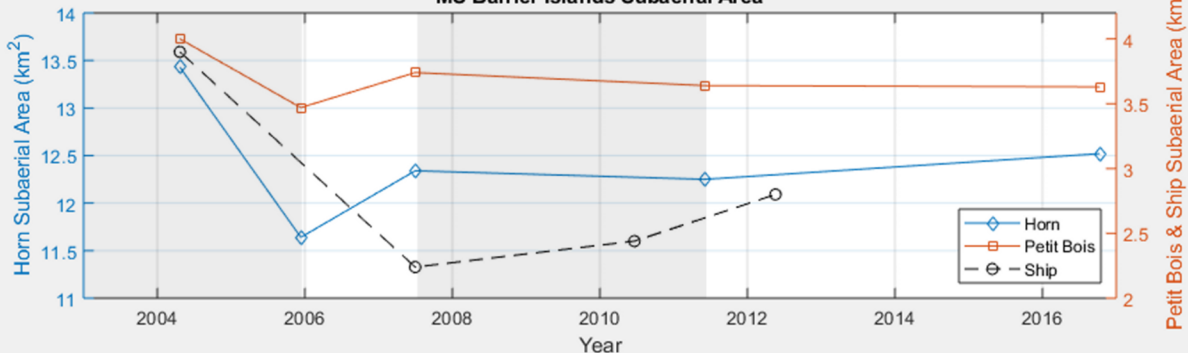
Horn Island Area Over Time



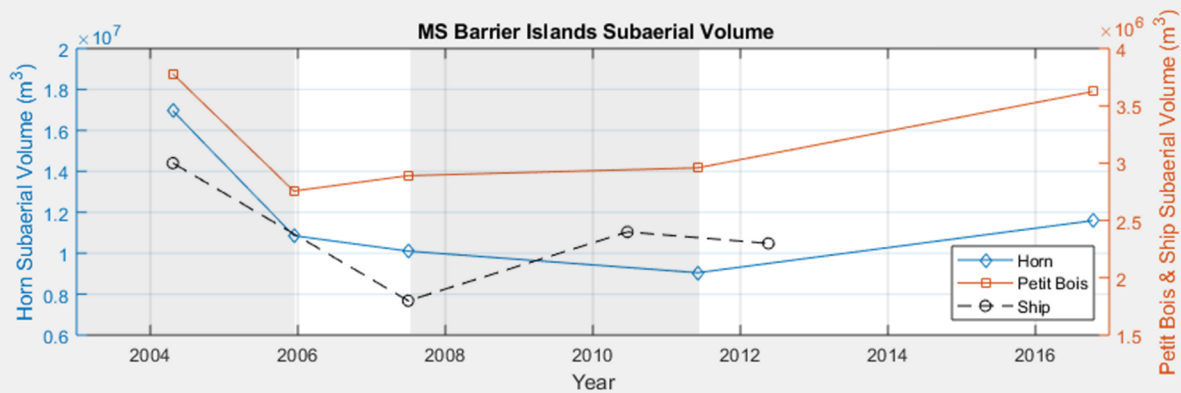
Petit Bois Island Area Over Time



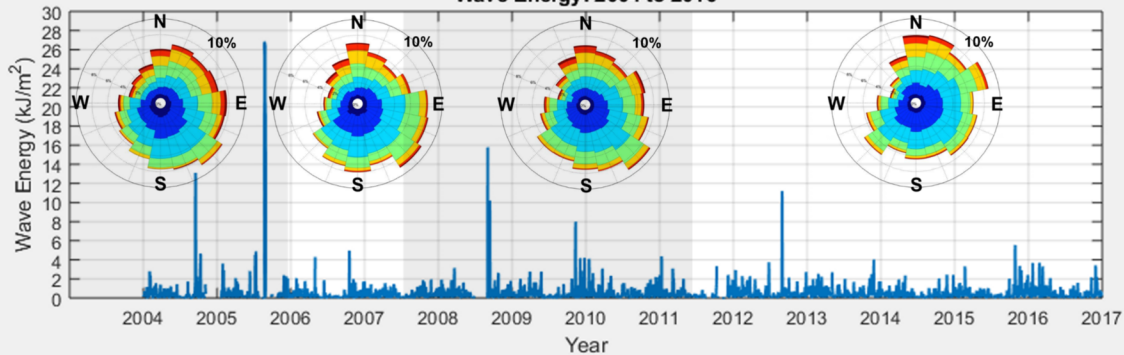
MS Barrier Islands Subaerial Area



MS Barrier Islands Subaerial Volume



Wave Energy: 2004 to 2016



Year	Dates	Name	Category (Cat) at landfall	Tropical Cyclone Summary	Pre-/Post-Storm Datasets	Data Sources
2004	2-24 Sept	Ivan	Cat 3 Hurricane	Landfall west of Gulf Shores, AL on 16 Sept.; ~194 kph winds. Horn & Petit Bois sustained 1-2 m storm surge.	2004, 2005	Stewart, 2004
2005	8-14 June	Arlene	Tropical Storm (TS)	Landfall at AL-FL stateline on 11 June; ~93 kph winds. Storm tide of ~0.8 m reported at Dauphin Island, AL.	2004, 2005	Avila & Brown, 2005
2005	3-11 July	Cindy	Cat 1 Hurricane	First landfall as a Cat 1 at 0300 UTC on 6 July southwest of Grand Isle, LA. Second landfall as a TS (~75 kph winds) near Ansley, MS at 0900 UTC. ~2 m storm surge recorded in Ocean Springs, MS.	2004, 2005	Stewart, 2006
2005	4-13 July	Dennis	Cat 3 Hurricane	Landfall as a Cat 3 on Santa Rosa Island, FL on 10 July; maximum sustained winds ~195 kph. Storm surge of 0.7-0.8 m and TS-force wind gusts 62-74 kph affected the study area.	2004, 2005	Beven, 2005
2005	23-31 Aug	Katrina	Cat 3 Hurricane	Landfall as a Cat 1 in southeast FL on 25 Aug. Second landfall near Buras, LA, as a Cat 3; maximum sustained winds ~204 kph at 1110 UTC on 29 Aug. Third landfall 3 hours later near LA-MS stateline; winds ~194 kph. Storm surges along coastal MS were >10 m.	2004, 2005	Knabb et al., 2005; Fritz et al., 2007
2009	4-10 Nov	Ida	Extra Tropical Cyclone (ETC)	Landfall as an ETC on Dauphin Island, AL on 10 Nov. ~1200 UTC. The preceding 12 hours, Ida was a TS; sustained winds 74 kph and gusts up to 94 kph. Storm surge at Pascagoula, MS was 0.97 to 1.09 m.	2007, 2011	Avila & Cangialosi, 2010
2011	2-5 Sept	Lee	Tropical Storm (TS)	Landfall on 4 Sept., ~27.5 km southeast of Ester, LA; 74 kph winds. Tracking through central and southeastern LA, winds decreased to ~65 kph for 18 hours. As Lee moved across southern MS, winds accelerated to 74 kph. Storm surge along coastal MS was 0.9 to 1.9 m.	2007, 2016	Brown, 2011
2012	21 Aug - 1 Sept	Isaac	Cat 1 Hurricane	First landfall on 29 Aug. at 0000 UTC on MS River's Southwest Pass, then at 0800 UTC in Port Fourchon, LA; maximum sustained winds ~130 kph. Isaac caused up to 0.56 m of rainfall along coastal MS and storm surges up to 2.4 m.	2011, 2016	Berg, 2013

LIDAR Dataset*	Date	Agency	Horizontal Uncertainty	Vertical Uncertainty	Elevation Coverage
NCMP Topobathy Lidar: Gulf (AL, FL, MS) & Atlantic Coast (NC)	April 2004	USACE	100 cm	15 cm (RMSE)	Topographic
NCMP Topobathy Lidar: Post Katrina (LA to FL)	December 2005	USACE	75 cm	20 cm (RMSE)	Topographic
Coastal Lidar: Northern Gulf (LA to FL)	June 2007	USGS	100 cm	15 cm (RMSE)	Topographic, Bathymetric
NCMP Topobathy Lidar: Gulf Coast (AL, MS, LA)	June 2011	USACE	75 cm	20 cm (RMSE)	Topographic
NCMP Topobathy Lidar: Gulf Coast (TX, MS, AL, FL)	October 2016	USACE	100 cm	10 cm (RMSE)	Topographic, Bathymetric

	24-hour Mean Wave Energy (kJ/m²)	Maximum Wave Energy (kJ/m²)	Date of Max	Cause of Max
P1: Jan. 1, 2004 - Dec. 31, 2005	0.485 ± 1.44	26.6 ^A	Aug. 29, 2005	Hurricane Katrina
P2: Jan 1, 2006 - Jul. 31, 2007	0.342 ± 0.48	4.97	Oct. 16, 2006	Squall Line
P3: Aug. 1, 2007 - Jun. 30, 2011	0.455 ± 0.76	15.79	Sept. 1, 2008	Hurricane Gustav
P4: Jul. 1, 2011 - Dec. 31, 2016	0.436 ± 0.60	11.2	Aug. 28, 2012	Hurricane Isaac
P5: Jan. 1, 2004 - Dec. 31, 2016	0.423 ± 0.80	26.6	Aug. 29, 2005	Hurricane Katrina

	Total Area (km²)	Areal Change (km²)	Total Average Shoreline Change Rate (m/yr)
2004	13.43		
		-1.79	-10.02
2005	11.64		
		+0.70	+4.16
2007	12.34		
		-0.09	-1.88
2011	12.25		
		+0.27	-0.83
2016	12.52		
Net Difference:		-0.91	
Average Rate of Change:		-0.07 km²/yr	-2.02 m/yr

	Total Volume (m ³)	Volume Change (m ³)
2004	1.695 x 10 ⁷	
		-6.09 x 10 ⁶
2005	1.086 x 10 ⁷	
		-0.76 x 10 ⁶
2007	1.01 x 10 ⁷	
		-1.05 x 10 ⁶
2011	0.905 x 10 ⁷	
		+2.54 x 10 ⁶
2016	1.159 x 10 ⁷	
Net Difference:		-5.36 x 10 ⁶
Average Rate of Change:		-4.29 x 10 ⁵ m ³ /yr

	Bathymetric Water Volume (m³)	Sediment Volume Change (m³)
2007	9.065 x 10 ⁶	
		-3.97 x 10 ⁵
2016	9.462 x 10 ⁶	

	Total Area (km²)	Areal Change (km²)	Total Average Shoreline Change Rate (m/yr)
2004	4.00		
		-0.53	-32.6
2005	3.47		
		+0.27	+5.15
2007	3.74		
		-0.10	-2.68
2011	3.64		
		-0.01	-1.47
2016	3.63		
Net difference:		-0.37	
Average Rate of Change:		-0.03 km²/yr	-3.14 m/yr

	Total Volume (m³)	Volume Change (m³)
2004	3.778 x 10 ⁶	
		-1.021 x 10 ⁶
2005	2.757 x 10 ⁶	
		+1.34 x 10 ⁵
2007	2.891 x 10 ⁶	
		+0.68 x 10 ⁵
2011	2.959 x 10 ⁶	
		+6.65 x 10 ⁵
2016	3.624 x 10 ⁶	
Net difference:		-1.54 x 10⁵
Average Rate of Change:		-1.23 x 10⁴ m³/yr

	Bathymetric Water Volume (m³)	Sediment Volume Change (m³)
2007	9.236 x 10 ⁶	
		+1.164 x 10 ⁶
2016	8.072 x 10 ⁶	
